

AD

Research and Development Technical Report

ECOM-0021-F

0  
G  
1  
0  
2  
1  
0  
7  
2  
0  
1  
0  
A  
P  
E

**MULTIPLE DOPED  
ERBIUM LASER MATERIALS**

**FINAL REPORT**

**Richard F. Woodcock**

**August 1971**

**Sponsored by  
Advanced Research Projects Agency  
ARPA, Order No. 1464**

D D C  
REPRODUCED  
AUG 18 1971  
RECEIVED  
B

**DISTRIBUTION STATEMENT**

**Approved for public release; distribution unlimited.**

**ECOM**

UNITED STATES ARMY ELECTRONICS COMMAND · FORT MONMOUTH, N.J.

CONTRACT DAAB07-<sup>70</sup>C-0021  
AMERICAN OPTICAL CORPORATION  
SOUTHBRIIDGE, MASSACHUSETTS 01550

Reproduced by  
**NATIONAL TECHNICAL  
INFORMATION SERVICE**  
Springfield, Va. 22151

**MISSING PAGE  
NUMBERS ARE BLANK  
AND WERE NOT  
FILMED**

## NOTICES

### Disclaimers

The findings in this report are not to be construed as an official Department of the Army position, unless so designated by other authorized documents.

The citation of trade names and names of manufacturers in this report is not to be construed as official Government indorsement or approval of commercial products or services referenced herein.

### Disposition

Destroy this report when it is no longer needed. Do not return it to the originator.

ACCESSION FOR	
CFSTI	WHITE SECTION <input checked="" type="checkbox"/>
DDC	BUFF SECTION <input type="checkbox"/>
UNARMED	<input type="checkbox"/>
DISPOSITION	
REASON FOR DISPOSITION	
CLASSIFICATION	
DATE ISSUED/AVAILABILITY CODES	
REF.	AVAIL. AND/or SPECIAL
A	

Unclassified

Security Classification

DOCUMENT CONTROL DATA - R & D

(Security classification of title, body of abstract and indexing annotation must be entered when the overall report is classified)

1. ORIGINATING ACTIVITY (Corporate author) American Optical Corporation Central Research Laboratory Southbridge, MA 01552	2a. REPORT SECURITY CLASSIFICATION Unclassified
	2b. GROUP N/A

3. REPORT TITLE

MULTIPLE DOPED ERBIUM LASER MATERIALS

4. DESCRIPTIVE NOTES (Type of report and Inclusive dates)  
Final Report - 1 Nov. 69-31 Jan. 71

5. AUTHOR(S) (First name, middle initial, last name)

Richard F. Woodcock

6. REPORT DATE August 1971	7a. TOTAL NO. OF PAGES 36	7b. NO. OF REFS 10
8. CONTRACT OR GRANT NO. DAAB07-70-C-0021	9a. ORIGINATOR'S REPORT NUMBER(S)	
b. PROJECT NO. 7910.21.702.55.01	9b. OTHER REPORT NO(S) (Any other numbers that may be assigned this report) ECOM-0021-F	
c.	d.	

10. DISTRIBUTION STATEMENT

Approved for public release; distribution unlimited.

11. SUPPLEMENTARY NOTES Sponsored by Advanced Research Projects Agency-ARPA, Order No. 1464	12. SPONSORING MILITARY ACTIVITY U.S. Army Electronics Command Fort Monmouth, N.J. 07703 AMSEL-KL-SM
--	---

13. ABSTRACT  
This report delineates efforts carried out under Contract No. DAAB07-70-C-0021, "Multiple Doped Erbium Laser Glasses." It presents the information in four sections. First, the program is introduced and gives some historical results from earlier company funded programs. The second section deals with the laser material improvement program and covers efforts concerned with optimizing both the core and cladding glasses. Closing section two is a discussion concerning possible advantages that could be obtained by varying the physical laser parameters. Section three presents experimental data and analysis of  $Er^{3+}$  site studies. Included are the effect of different sites upon the  $Er^{3+}$  emission spectra in glass, studies of various glasses with enhanced emission of 1536 nm and studies of the crystal field splitting of  $Er^{3+}$  in the near octahedral A site. Finally, a summary and some conclusions are presented.

Unclassified

Security Classification

14. KEY WORDS	LINK A		LINK B		LINK C	
	ROLE	WT	ROLE	WT	ROLE	WT
Lasers Glass Lasers Erbium Lasers Erbium Doped Glass Glass Cladding Sensitizing Agents Rare Earth Oxides						

Unclassified

Security Classification

  
TECHNICAL REPORT ECOM-0021-F

REPORTS CONTROL SYMBOL  
OSD-1366

MULTIPLE DOPED ERBIUM LASER MATERIALS

FINAL REPORT

1 November 1969 - 31 January 1971

Contract DAAB07-70-C-0021  
DA Project No. 7910.21.702.55.01

Prepared By

Richard F. Woodcock  
American Optical Corporation  
Southbridge, MA 01550

For

United States Electronic Command  
Fort Monmouth, N.J.

DISTRIBUTION STATEMENT

Approved for public release; distribution unlimited.

## ABSTRACT

This report delineates efforts carried out under Contract No. DAAB07-70-C-0021, "Multiple Doped Erbium Laser Glasses." It presents the information in four sections. First, the program is introduced and gives some historical results from earlier company funded programs. The second section deals with the laser material improvement program and covers efforts concerned with optimizing both the core and cladding glasses. Closing section two is a discussion concerning possible advantages that could be obtained by varying the physical laser parameters. Section three presents experimental data and analysis of  $\text{Er}^{3+}$  site studies. Included are the effect of different sites upon the  $\text{Er}^{3+}$  emission spectra in glass, studies of various glasses with enhanced emission of 1536 nm and studies of the crystal field splitting of  $\text{Er}^{3+}$  in the near octahedral A site. Finally, a summary and some conclusions are presented.

## FOREWORD

The efforts reported herein were accomplished under Contract No. DAAB07-70-C-0021, Project No. 7910.21.702.55.01 for the Microwave and Quantum Electronics Branch of the Solid State and Frequency Control Division of the Electronics Components Laboratory, U. S. Army Electronics Command, Fort Monmouth, New Jersey. Contractors representatives were Dr. E. Schiel and Mr. V. Kublin.

The work was carried out by the Basic Materials Research Department at the Central Research Laboratory of the American Optical Corporation in Southbridge, Massachusetts under the direction of Dr. Richard F. Woodcock. Dr. Charles C. Robinson provided experimental and theoretical analysis of Er<sup>3+</sup> Site Studies found in Section 3.

This research was supported by the Advances Research Projects Agency of the Department of Defense and was monitored by the U. S. Army Electronics Command under Contract Number DAAB07-70-C-0021.

This report is the final report under this contract and is unclassified.

## TABLE OF CONTENTS

	PAGE
1. INTRODUCTION . . . . .	1
2. LASER MATERIAL IMPROVEMENT PROGRAM . . . . .	3
2.1 OPTIMIZATION OF $\text{Er}_2\text{O}_3$ CONCENTRATION IN CORE GLASS . . .	4
2.2 OPTIMIZATION OF CLADDING GLASS . . . . .	8
2.3 LASER ROD DIMENSION . . . . .	17
3. $\text{Er}^{3+}$ SITE STUDIES . . . . .	18
3.1 THE EFFECT OF DIFFERENT SITES UPON THE $\text{Er}^{3+}$ EMISSION SPECTRA IN GLASS	18
3.2 GLASSES WITH ENHANCED EMISSION AT 1536 nm . . . . .	25
3.2.1 RARE EARTH - SILICATE GLASSES . . . . .	25
3.2.2 PHOSPHATE GLASSES . . . . .	27
3.2.3 GERMANATE AND BORATE GLASSES . . . . .	29
3.3 THE CRYSTAL FIELD SPLITTING OF $\text{Er}^{3+}$ IN THE NEAR OCTAHEDRAL A SITE	30
4. SUMMARY AND CONCLUSIONS . . . . .	34

## ILLUSTRATIONS

FIGURE	PAGE
1. Photographs of "standard" laser test system.	5
2. Laser threshold as a function of $\text{Er}_2\text{O}_3$ concentration.	7
3. Typical laser performance curves.	7
4. Slope efficiency as a function of $\text{Er}_2\text{O}_3$ concentration.	9
5. Energy required for 50 mJ output vs $\text{Er}_2\text{O}_3$ concentration.	9
6. Input energy required for 100 mJ output vs cladding thickness.	11
7. Input energy required for 100 mJ output vs cladding thickness of $\text{Cr}^{3+}$ -cladding glasses.	16
8. Input energy required for 100 mJ output vs cladding thickness of $\text{U}^{6+}$ -cladding glasses.	16
9. Low temperature $^4\text{I}_{15/2} - ^4\text{S}_{3/2}$ spectra.	20
10. Room temperature $^4\text{I}_{13/2} - ^4\text{I}_{15/2}$ $\text{Er}^{3+}$ emission spectra.	23
11. The energies corresponding to the spectral peaks in the $^4\text{I}_{15/2}$ absorption and emission spectra of $\text{Er}^{3+}$ in the A site.	24
12. Room temperature $^4\text{I}_{13/2} - ^4\text{I}_{15/2}$ $\text{Er}^{3+}$ emission spectra.	26
13. Low temperature $^4\text{I}_{15/2} - ^4\text{S}_{3/2}$ $\text{Er}^{3+}$ absorption spectra in a zinc alumina phosphate glass.	27
14. Room temperature $^4\text{I}_{13/2} - ^4\text{I}_{15/2}$ $\text{Er}^{3+}$ emission spectra in a zinc alumina phosphate glass.	28

## ILLUSTRATIONS

FIGURE		PAGE
15.	Room temperature $^4I_{13/2} - ^4I_{15/2}$ Er <sup>3+</sup> emission spectra in a barium metaphosphate glass.	28
16.	Low temperature $^4I_{15/2} - ^4S_{3/2}$ absorption spectra.	29
17.	The low temperature A site $^4I_{15/2} - ^4I_{9/2}$ Er <sup>3+</sup> absorption spectrum.	32
18.	The low temperature A site $^4I_{15/2} - ^4I_{11/2}$ Er <sup>3+</sup> absorption spectrum.	32
19.	The low temperature A site $^4I_{15/2} - ^4I_{13/2}$ Er <sup>3+</sup> absorption spectrum.	33
20.	The low temperature A site $^4I_{13/2} - ^4I_{15/2}$ Er <sup>3+</sup> emission spectrum.	33

TABLES	PAGE
I. Effect of Er <sub>2</sub> O <sub>3</sub> Concentration on Laser Performance	6
II. Sensitizer Content of Cladding Glasses	10
III. Effect of Sensitizing Agents on Yb <sup>3+</sup> Fluorescent Intensity	14
IV. Effect of Cavity Parameters on Laser Performance	17
V. Merit Factor $I_{1536}\alpha_{1543}/I_{1543}\alpha_{1536}$ For Various Glasses	25
VI. Operator Equivalent Factor for Er <sup>3+</sup>	31

## MULTIPLE DOPED ERBIUM MATERIALS

### 1. INTRODUCTION

This report covers work performed under Contract No. DAAB07-70-C-0021. The original contract was for a 12 month effort ending 31 October 1970. At the suggestion of the contracting agency, the preparation of the final report was postponed for three months in order that the results of work still in progress at the end of the 12 month period might be included in the final report. The goal of the work performed under this contract was to investigate the possibility of improving the performance of an erbium laser system by physically separating the sensitizing portion of a rod from the active laser region.

Previous work on multiple doped erbium lasers indicated that the material was most efficient when neodymium and ytterbium were added to the glass. The former serves as a sensitizing agent by absorbing pump light in the visible regions of the spectrum where the  $\text{Er}^{3+}$ -ion is a relatively poor absorber. The  $\text{Yb}^{3+}$ -ion serves as an agent for transferring energy from the  $\text{Nd}^{3+}$ -ion to the  $\text{Er}^{3+}$ -ion. The  $\text{Yb}^{3+}$ -ion also serves as a strong sensitizing agent in the near infrared region of the spectrum. The presence of  $\text{Nd}^{3+}$ -ions in the active laser region can have a competing detrimental effect on laser performance, since quenching of the  $\text{Er}^{3+}$ -ion may occur by a transfer of energy from the  $^4\text{I}_{13/2}$  level of the  $\text{Er}^{3+}$ -ion to the  $^4\text{I}_{15/2}$  level of the  $\text{Nd}^{3+}$ -ion. There is also a small amount of absorption at the  $1.54 \mu\text{m}$  emission wavelength resulting from the wings of a neodymium absorption band at  $1.06 \mu\text{m}$ . These effects limited the amount of  $\text{Nd}_2\text{O}_3$  which could be used to advantage in a homogeneously doped material to a few tenths of one percent.

The present work is an outgrowth of a company funded effort to physically separate the functions of the neodymium sensitizing ion and the erbium laser ion, the results of which showed good promise for a system with potentially higher overall laser efficiency in the 50 to 100 mJ output range. This higher overall efficiency was obtained by a combination of a decrease in laser threshold and an increase in the slope efficiency above laser threshold. This is achieved by using a composite laser rod consisting of a cylindrical core of active laser glass, containing  $\text{Er}^{3+}$ - and  $\text{Yb}^{3+}$ -ions, which is clad with a sleeve of sensitizing glass containing  $\text{Nd}^{3+}$ - and  $\text{Yb}^{3+}$ -ions. In this

configuration, the  $\text{Nd}^{3+}$ -ions are in general far enough away from the  $\text{Er}^{3+}$ -ions to prevent quenching of the latter. Since the laser light does not pass through the  $\text{Nd}^{3+}$ -containing glass, the cavity loss due to the absorption in the short wavelength wing of the  $1.6 \mu\text{m}$   $\text{Nd}^{3+}$ -absorption line is eliminated. The latter system has the potential advantages that; (1) higher concentrations of sensitizer ions might be used, (2) additional sensitizing agents which might otherwise adversely affect the  $\text{Er}^{3+}$ -ions may also be used, (3) an antisolarizing agent can be added to the cladding to protect the active core glass without effecting its laser properties and, (4) the laser rod configuration might be designed to reduce thermal distortion in the active core of the laser rod since the majority of the pumping processes occur in the cladding glass rather than in the core glass.

Although the results of previous studies on unclad erbium systems indicate that phosphate glasses gave better results than silicate glasses, the present effort on clad erbium systems was carried out with silicate based glasses. The main reason for this is that the silicate based glasses tend to give more reproducible results from one melt to the next because of their better glass making characteristics. Thus, although the phosphate materials may have greater ultimate potential it was felt that the development of clad erbium systems could be carried out in a more expedient manner and with a higher probability of success using the silicate based materials in which erroneous data due to spurious effects from one melt to the next are kept to a minimum.

The present studies to optimize clad erbium laser rod performance included efforts to; (1) optimize the concentration of the active  $\text{Er}^{3+}$ -ion in the core glass and the  $\text{Nd}^{3+}$ - and  $\text{Yb}^{3+}$ -sensitizing ions in the cladding glass, (2) incorporate additional sensitizing elements in the cladding glass and optimize their concentrations, (3) add antisolarizing agents in the cladding glass and (4) determine the effects of laser rod parameters such as cladding thickness and laser rod dimensions on laser performance. In addition, an investigation was carried out on the effect of host glass composition on the lattice site of the  $\text{Er}^{3+}$ -ion.

Most of the experimental glass melts for the clad rod studies were made in platinum crucibles which expedites the glass fabrication process, but results in a material which may not be suitable for applications in which high energy densities of laser light are encountered such as lasing in the Q-switched mode. To satisfy the latter conditions some melts were also made in ceramic crucibles. Representative samples of both

platinum and ceramic melted glasses were supplied to the contracting agency for further evaluation.

## 2. LASER MATERIAL IMPROVEMENT PROGRAM

Individual aspects of the program designed to improve the laser performance of clad erbium rods will be treated separately in following sections. An attempt was made to standardize the general procedure for fabricating and testing clad rods as much as possible so that valid comparisons of results could be made.

The fabrication of experimental glasses was in general carried out in platinum crucibles. The size of the melts varied from about 0.4 to 7.0 kilograms. Smaller melts (0.4-0.9 kg) were made of glasses in which a particular parameter was being systematically varied, such as the erbium concentration in the core glass or the sensitizing agent in the cladding glass. For the core glass studies extra effort was made to provide glasses of reasonably good optical homogeneity. Although reasonable success was achieved by paying careful attention to stirring procedures and the time-temperature cycles of the melt, the quality of small melts cannot be expected to be as good as that in larger melts. Variations in optical quality of the core glass can be expected to change values of slope efficiency above threshold but tend to have much less effect on the value of laser threshold itself. The larger melts of glass are used for the rod component which remains unchanged in a given study, for example, the core glass in a study of the effect of sensitizing agents in the cladding glass. In this way variations due to the core glass are kept to a minimum, since all of the core material for a given set of cladding experiments may come from the same glass melt.

The laser rods are fabricated by making a tube of the cladding material, 20-25 mm OD with an ID about half that diameter, into which a solid cylinder of core material is placed such that the assembly may be heated and drawn down into a fused clad rod with an 8 mm cladding diameter and a 4 mm core diameter. The surfaces of the core to cladding interface are polished prior to assembly and drawing. The composition of the base glass for both core and cladding materials are essentially the same. Some adjustment in composition is necessary, however, to compensate for the difference in expansion coefficient of these two materials which occurs as a result of differences in their rare earth concentrations, i.e. about 15 wt % in the core glass versus 5 to 10 wt % in the cladding glass. This is done by adding  $\text{Y}_2\text{O}_3$  to

the cladding glass to make up for its lower rare earth concentration.

Measurement of laser threshold energies and slope efficiencies are carried out using the "standard" laser cavity shown in Figure 1. The primary consideration in the design of this cavity was ease of performing laser measurements and their reproducibility rather than optimum laser performance. The measurements were in general carried out on laser rods with an 8 mm cladding diameter, a 4 mm core diameter and a 76 mm length. Optical pumping was provided by two xenon-filled flashlamps, with 6 mm OD - 4 mm ID quartz envelopes connected in series through an inductance of 4460  $\mu$ H to a power supply with a 760  $\mu$ F storage capacitance. Output from the flashlamps is coupled to the laser rod by a close wrap of silver foil. End mirrors for the cavity are a nominal 100 percent and 65 percent reflectivity. The above parameters exist for all the following measurements unless otherwise specified. The composition of the base glass to which the various laser and sensitizing ions are added is approximately; 70.6 wt %  $\text{SiO}_2$ , 1.0 wt %  $\text{Li}_2\text{O}$ , 7.6 wt %  $\text{Na}_2\text{O}$ , 11.5 wt %  $\text{K}_2\text{O}$ , 5.0 wt %  $\text{BaO}$ , 1.1 wt %  $\text{Sb}_2\text{O}_3$ , 1.6 wt %  $\text{ZnO}$  and 1.6 wt %  $\text{Al}_2\text{O}_3$ .

## 2.1 OPTIMIZATION OF $\text{Er}_2\text{O}_3$ CONCENTRATION IN CORE GLASS

In order to determine the optimum concentration of the active laser ion in the core glass a series of core glasses was melted which contains from 0.15 wt % to 1.0 wt %  $\text{Er}_2\text{O}_3$  as the active laser ion and approximately 15 wt %  $\text{Yb}_2\text{O}_3$  as a transfer agent. The cladding glass, MG-2400, has the same base composition as the core glass, but contains 4 wt %  $\text{Nd}_2\text{O}_3$ , 4 wt %  $\text{Yb}_2\text{O}_3$ , and 1.9 wt %  $\text{CeO}_2$ . The  $\text{Nd}^{3+}$ - and  $\text{Yb}^{3+}$ -ions serve as sensitizing agents for the core glass and the  $\text{Ce}^{3+}$ -ion is added primarily as an antisolarizing agent, but may also serve as a sensitizing agent.

Measurement of laser threshold and slope efficiency above threshold were made in the laser cavity described in Section 2. Measurements were made using an 80 percent output reflector in addition to the 65 percent output reflector normally used. Results of these measurements made on laser rods with a fine ground cylindrical surface are given in Table I.

The core glasses were made in 0.4-0.9 kilogram melts with the exception of the 0.3 wt %  $\text{Er}_2\text{O}_3$  glass, MG-2101 G which was a 4.0 kilogram melt made in a ceramic crucible, as was the glass with which it was clad, MG-2400A. The cladding material for these glasses was taken from the same melt of glass, MG-2400 B,

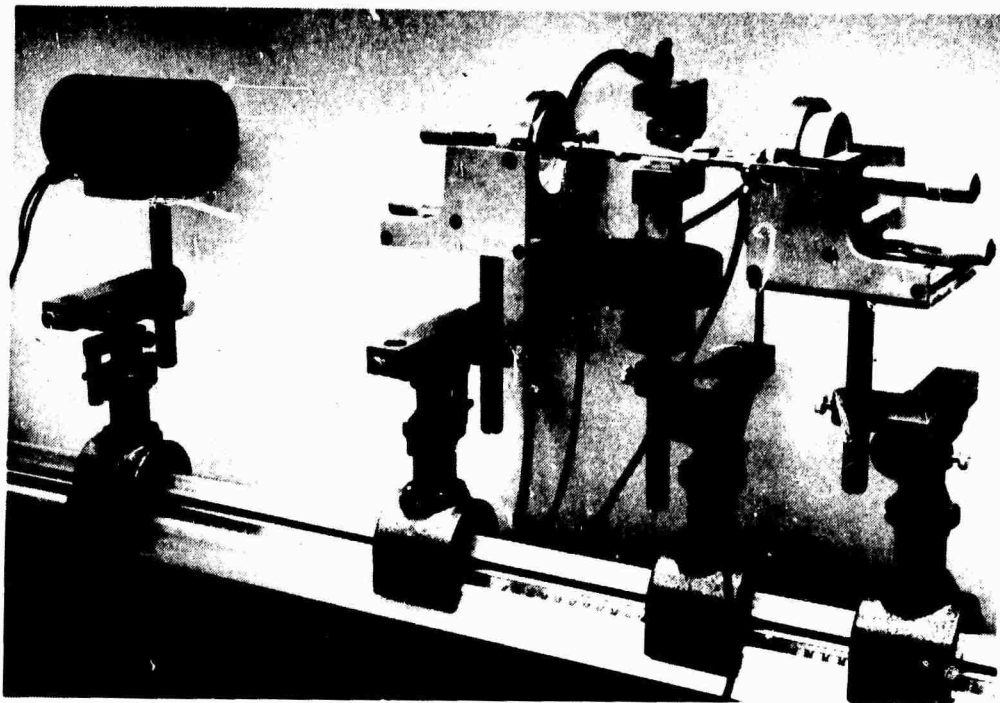


Figure 1. Photographs of "standard" laser test system.  
(a) Flashlamp and rod assembly, end mirrors  
and thermopile detector on optical bench with  
mounts to provide desired degrees of motion.  
(b) Flashlamp and laser rod arrangement prior  
to close-wrapping with silver foil.

with the exception of the above glass melted in ceramic and the cladding glass for the 0.7 wt %  $\text{Er}_2\text{O}_3$ , glass (MG-2499A), a member of the series which had to be remelted; thus, this laser rod was fabricated sometime after the rest of the series. Values of the erbium concentrations in Table I given in parenthesis are corrected values of the nominal  $\text{Er}_2\text{O}_3$  concentration, calculated from the absorption peak at 518 nm and normalized to the 0.3 wt % value. The point of normalization is an arbitrary one and was chosen on the basis that this seven kilogram melt represents the largest absolute amount of  $\text{Er}_2\text{O}_3$  added to any of the above melts of glass and therefore, presumably has the lowest percentage of error in batch composition.

TABLE I. Effect of  $\text{Er}_2\text{O}_3$  Concentration  
on Laser Performance

		$\text{Er}_2\text{O}_3$ Conc. Wt % (corrected values)	Laser Threshold (Joules) R=80% R=65%		Laser Slope Efficiency R=80% R=65%	
MG-2110A	MG-2400B	1.0 (0.965)	365	350	0.29	0.33
MG-2499A	MG-2400C	0.7 (0.69)	225	237	0.43	0.55
MG-2495A	MG-2400B	0.5 (0.495)	162	175	0.36	0.49
MG-2453A	MG-2400B	0.25 (0.27)	130	145	0.27	0.37
MG-2450A	MG-2400B	0.2 (0.18)	108	123	0.18	0.16
MG-2430A	MG-2400B	0.15 (0.155)	95	125	0.09	0.08
MG-2445A	MG-2400B	0.1 (0.077)	100	190	0.05	0.04
MG-2101G <sup>a</sup>	MG-2400A <sup>a</sup>	0.3 (0.30)	135	155	0.19	0.27

<sup>a</sup>4.5 kg melt made in ceramic crucible.

Figure 2 is a plot of the threshold energy required for laser action as a function of corrected  $\text{Er}_2\text{O}_3$  concentration for both a 65 percent and an 80 percent front reflector. A typical curve from which values of threshold and efficiency are obtained is shown in Figure 3. The error bars in Figure 2 (and Figures 4 and 5) represent the accuracy with which the various parameters are extracted from the data depicted in Figure 3 and does not take into consideration variations which exist in the experimental setup such as varying degrees of stria in the core glass, deterioration of cavity components, etc. As indicated in Figure 2 the

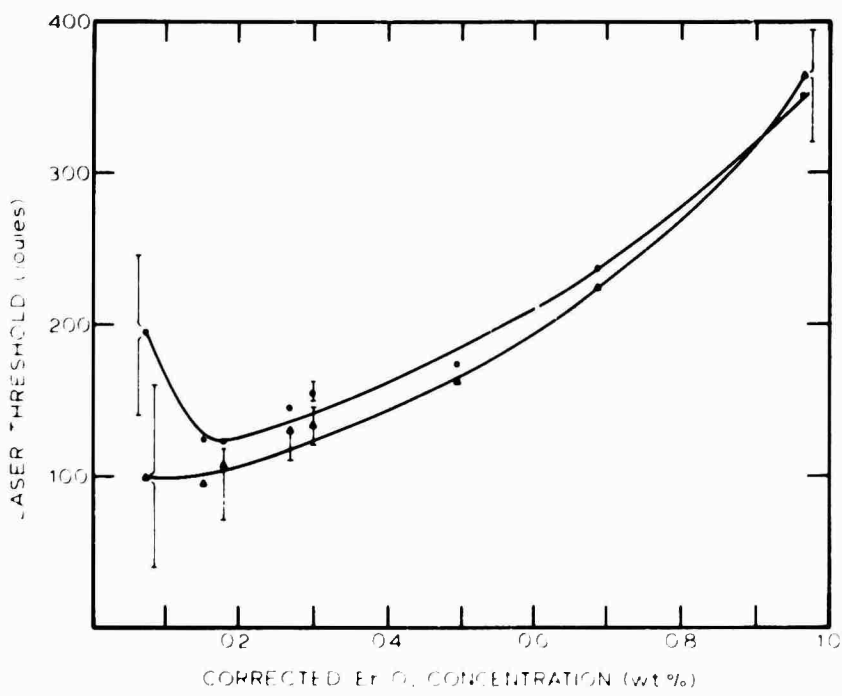


Figure 2. Laser threshold as a function of  $\text{Sr}_2\text{O}_3$  concentration.

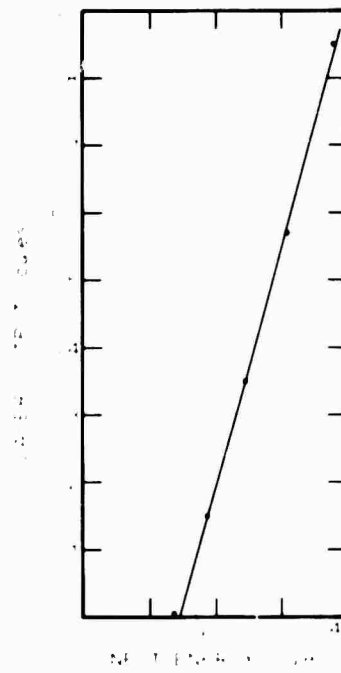


Figure 3. Typical laser performance curve.

minimum threshold appears to occur for  $\text{Er}_2\text{O}_3$  concentrations in the 0.15-0.2 wt % region for a 65% output reflector. Not only is the laser threshold lower for the 80% reflectivity output mirror, but it also appears to occur at a lower concentration of  $\text{Er}_2\text{O}_3$ . The higher degree of uncertainty in threshold values for glasses with low  $\text{Er}_2\text{O}_3$  concentrations is due in part to the low slope efficiency of these rods as indicated in Figure 4, a plot of slope efficiency above threshold as a function of  $\text{Er}_2\text{O}_3$  concentration. That figure indicates that maximum slope efficiency is obtained for  $\text{Er}_2\text{O}_3$  concentrations in the 0.5-0.7 wt % region. The overall efficiency for a 50 mJ output is a function of both slope efficiency and laser threshold. As indicated in Figure 5, the minimum input energy required for 50 mJ output (optimum overall efficiency at 50 mJ) appears to occur in the 0.2-0.25 wt %  $\text{Er}_2\text{O}_3$  region, rising slowly for higher erbium concentrations and more abruptly at lower erbium concentrations.

The apparent low value of slope efficiency for the 0.3 wt % erbium glass cannot be attributed to poor optical quality, because this was from the 4 kilogram melt made in a ceramic crucible which generally gives very good optical quality. One possible explanation is that the ceramic crucible may introduce some contamination into the melt which provides a loss mechanism. To investigate this possibility, a laser rod was fabricated using the same ceramic melted core glass, but with a platinum melted cladding glass. This rod was found to have higher efficiency than a comparable rod in which both core and cladding glasses were melted in a ceramic crucible. The fact that the difficulty appears to occur in the cladding glass is not surprising since the slowest step, and thus the most vulnerable one in the chain of events leading to excitation of the  $\text{Er}^{3+}$ -ions, is the fluorescent emission from  $\text{Yb}^{3+}$ -ions in the cladding which is subsequently absorbed by the  $\text{Yb}^{3+}$ -ions in the core material.

## 2.2 OPTIMIZATION OF CLADDING GLASS

The optimization of the cladding glass falls into three general categories, namely: (1) optimization of the rare earth concentration in the cladding glass, (2) thickness of the cladding glass and (3) the addition of other beneficial ions in the cladding glass. Items 1 and 2 appear to be interrelated since together they determine the total number of rare earth ions in the cladding. A series of cladding glasses was prepared in which the  $\text{Nd}_2\text{O}_3$  and  $\text{Yb}_2\text{O}_3$  concentrations varied from 2-7 wt %. In addition to the sensitizing agents these glasses contained 1.9 wt %  $\text{CeO}_2$ , primarily as an antisolarizing agent for the glass. These compositions also

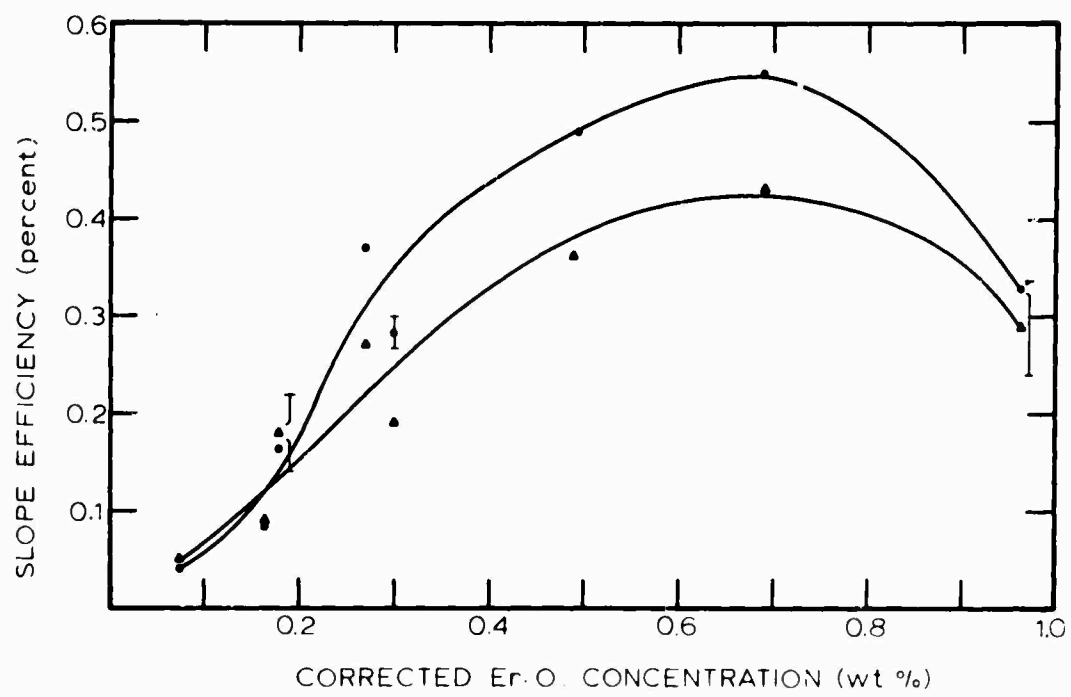


Figure 4. Slope efficiency as a function of  $\text{Er}_2\text{O}_3$  concentration.

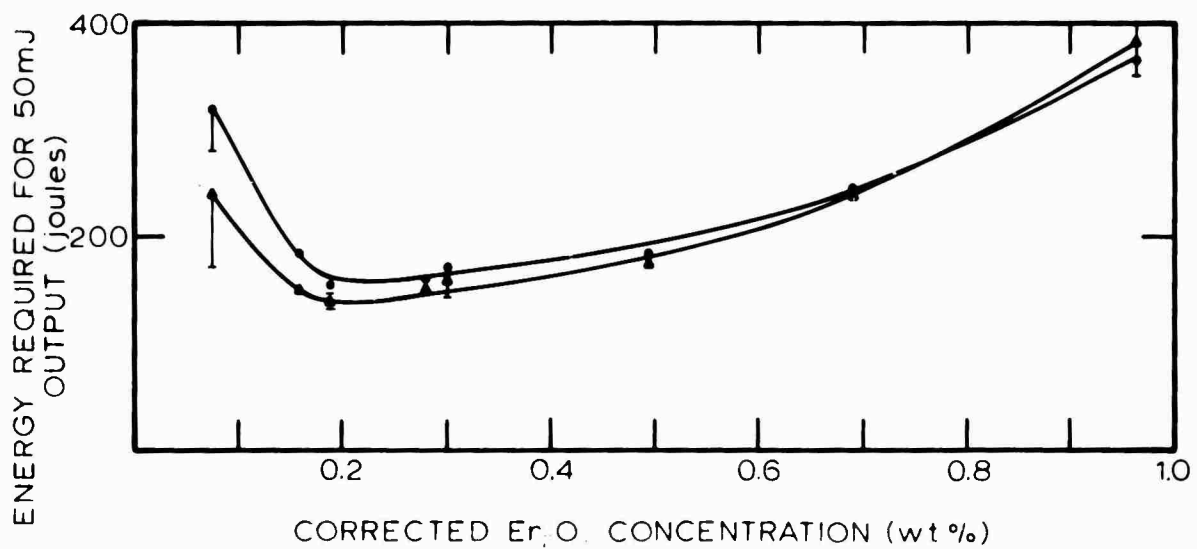


Figure 5. Energy required for 50 mJ output vs  $\text{Er}_2\text{O}_3$  concentration.

contained from 0 to 8 wt %  $\text{Y}_2\text{O}_3$  so that the expansion coefficient of the cladding glass would be compatible with that of the core glass. This requirement for the addition of  $\text{Y}_2\text{O}_3$  to compensate for differences in expansion coefficient and the approximate concentrations required were determined in a previous in-house project. The material for all of the core glasses in this series came from a single ten-pound melt of composition MG-2101, containing 15 wt %  $\text{Yb}_2\text{O}_3$  and 0.3 wt %  $\text{Er}_2\text{O}_3$ .

The rare earth concentrations of all the cladding glasses are given in Table II. Measurements of laser parameters were carried out in the laser cavity described in Section 2. The reflectivity of the output mirror was 65% in all cases. Laser measurements were made with cladding glass thicknesses of 2.0, 1.0, 0.75, 0.5, 0.25 and 0 mm. In general, the thickness measurements are first made on a rod with a 2 mm cladding thickness which is then reduced in the above steps by centerless grinding for subsequent measurements, thus eliminating any variations in the active core region of the laser rod. The cladding thickness was completely removed in the final step and the properties of just the core glass were measured in an attempt to provide a normalizing value. This was only partially successful since the glass shows some tendency toward solarization when all the protective cladding has been removed.

TABLE II. Sensitizer Content of Cladding Glasses

Glass Number	$\text{Nd}_2\text{O}_3$ (wt %)	$\text{Yb}_2\text{O}_3$ (wt %)	$\text{Cr}_2\text{O}_3$ (wt %)	$\text{UO}_2$ (wt %)	$\text{CeO}_2$ (wt %)
MG-2494	2	3			1.9
MG-2496	3	2			1.9
MG-2497	3	3			1.9
MG-2500	4	3			1.9
MG-2400	4	4			1.9
MG-2556	5	5			1.9
MG-2561	7	7			1.9
MG-2637	4	4	0.025		1.9
MG-2640	4	4	0.05		1.9
MG-2540	4	4	0.1		
MG-2518	4	4	0.25		
MG-2628	4	4		0.1	1.9
MG-2512	4	4		0.25	1.9
MG-2637	4	4		0.5	1.9

In all cases these cladding glasses were used with an MG-2101 core glass containing 0.3 wt %  $\text{Er}_2\text{O}_3$  and 15.0 wt %  $\text{Yb}_2\text{O}_3$ .

A series of curves is given in Figure 6 depicting the change in energy required for a 100 mJ output as a function of cladding thickness for the different cladding glasses. The effect of rare earth concentration in the cladding glass in general appears to be small for the range of concentrations investigated. An attempt has been made to draw a smooth curve through the data points although the scatter of experimental points makes this difficult in some cases. The error bars reflect the uncertainty of the 100 mJ output point obtained from a given slope efficiency curve and do not represent a statistical average since only one rod was measured in most cases. The abscissa in Figure 6 is labeled in relative cross-sectional area of the cladding as well as cladding thickness.

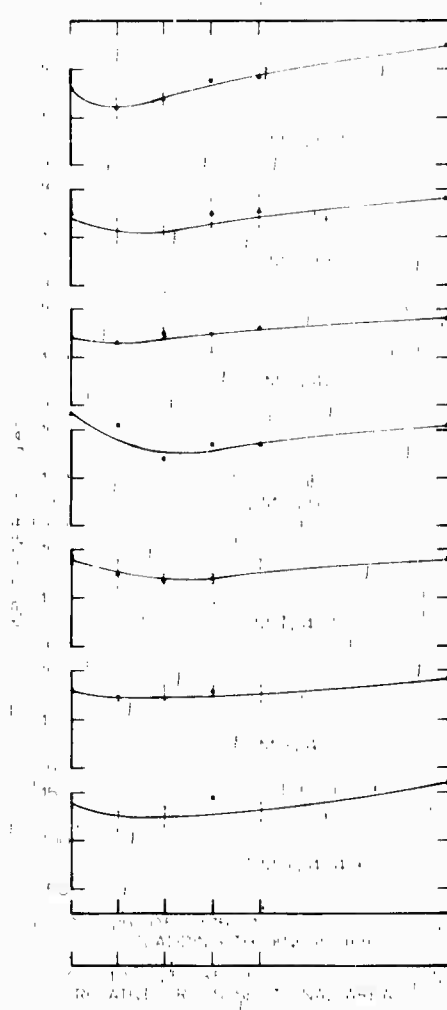


Figure 6. Input energy required for 100 mJ output vs cladding thickness.

The results would indicate that the sensitization is a function of the total number of sensitizing ions present assuming that the cladding thickness does not become excessive. Thus, based on the minimum in the curve for MG-2561 cladding containing 7 wt %  $\text{Yb}_2\text{O}_3$  one would expect the minimum for the rod clad with MG-2556 (5 wt %  $\text{Nd}_2\text{O}_3$ , 5 wt %  $\text{Yb}_2\text{O}_3$ ) to occur at a relative cross-sectional area of 1.2, that for glasses MG-2400 and MG-2500 (4 wt %  $\text{Nd}_2\text{O}_3$  and 4 and 3 wt %  $\text{Yb}_2\text{O}_3$  respectively) to occur at a relative cross-sectional area of approximately 1.75 and rods clad with MG-2497 (3 wt %  $\text{Nd}_2\text{O}_3$  and 3 wt %  $\text{Yb}_2\text{O}_3$ ) should have a minimum at a relative cross-sectional area of approximately 2.3. The actual minimum values appear to agree fairly well with those predicted on the basis of the number of rare earth ions in the cladding.

In order to take fullest advantage of optical immersion of the core by the cladding when the refractive index is about 1.5, the cladding thickness should be about one-half the radius of the core. For this reason it is advantageous in the present case where the core diameter is 4 mm not to exceed a 1 mm cladding thickness. Aside from the arguments for optical immersion, better efficiency should be obtained with a thin cladding of higher  $\text{Nd}_2\text{O}_3$  and  $\text{Yb}_2\text{O}_3$  concentration because the acceptance angle for light striking the core is greater for atoms located nearer the core and because the energy transfer between  $\text{Nd}^{3+}$ -ions and  $\text{Yb}^{3+}$ -ions is greater at the higher concentrations. This appears to be the case in the uncorrected, unnormalized data presented in Figure 6 where the greatest efficiencies, i.e. lowest input energies for 100 mJ of output, tend to occur for higher concentrations of  $\text{Nd}_2\text{O}_3$  and  $\text{Yb}_2\text{O}_3$  in the cladding.

Other additives to the cladding glass were also considered. One of these is the addition of  $\text{CeO}_2$  to the cladding glass to prevent solarization. Initial melts and subsequent testing of such a material were carried out under a company sponsored project. In that work, 4.5 kilogram melts were made of MG-2101 core glass and MG-2400 cladding glass compositions in ceramic crucibles and these were subsequently fabricated into clad erbium laser rods. A system containing a rod of this material showed no degradation in output after being fired 1000 times at an input of 150 joules. Results of this work, in which single Q-switched pulses of 55 mJ output in a 35 ms width were obtained at an input of 132 J, were reported at the San Diego DOD Conference on Laser Technology.<sup>1, 2</sup> In addition to its antisolarization properties, the  $\text{Ce}^{3+}$ -ion may also be serving as an additional sensitizing agent.

The fact that the sensitizing agents may be placed in the cladding glass makes it possible to consider the use of sensitizing agents which would be incompatible with the active portion of the laser due to quenching or absorption. To investigate this possibility, a series of cladding glasses were made containing 4 wt %  $\text{Nd}_2\text{O}_3$ , 4 wt %  $\text{Yb}_2\text{O}_3$  and varying amounts of  $\text{Cr}^{3+}$ ,  $\text{Mn}^{2+}$ ,  $\text{Mo}^{3+}$ ,  $\text{V}^{5+}$ , and  $\text{U}^{6+}$  ions. A preliminary evaluation of these potential cladding materials was made by measuring the energy transferred by these ions to the  $\text{Yb}^{3+}$ -ions. This is done by measuring the  $\text{Yb}^{3+}$ -fluorescent intensity of the material as a result of excitation from a high pressure mercury-vapor arc which had all wavelengths above approximately 800 nm removed by means of a heat screen filter so that no direct pumping of the  $\text{Yb}^{3+}$ -ion was allowed to occur.

The absolute measurement of fluorescent intensity is not a trivial one to perform. For this reason a standard sample was measured with each of the test samples as a reference. As indicated by the results tabulated in Table III, fluorescent emission from the standard sample was reproducible to about  $\pm 5\%$ . In order to take into account variations which may be due to the preparation of the sample, e.g. surface polish or variations in the  $\text{Yb}_2\text{O}_3$  concentration, an attempt was made to use the  $\text{Yb}^{3+}$ -ions in the glass as an "internal" reference. The approach taken was to excite just the  $\text{Yb}^{3+}$ -ions in the sample, by using a 970 nm narrow-bandpass filter on the pump source, and monitor the  $\text{Yb}^{3+}$ -ion emission. The resulting degree of variation in  $\text{Yb}^{3+}$ -ion emission is not a satisfactory reference because it is too strongly influenced in some cases by the other additives in the cladding glass.

The emission data, when compared to the MG-2400 composition on which these glasses were based, indicate that many of the additives tend to quench the  $\text{Yb}^{3+}$ -ion emission. For example, in the chromium series, as the concentration of  $\text{Cr}_2\text{O}_3$  is increased the emission intensity starts off equal to that of MG-2400 and then decreases. This is also the case for the uranium series. These results would also suggest that manganese and vanadium tend to quench the Yb fluorescence while molybdenum seems to have little effect. The difference in emission between MG-2400 and MG-2500 is in proportion to the lower concentration of  $\text{Yb}_2\text{O}_3$  in the latter glass. The higher Yb emission intensity for MG-2494 might be attributed to a decrease in quenching action by the lower  $\text{Nd}_2\text{O}_3$  concentration. The role that appears to be played by the  $\text{CeO}_2$  is not immediately obvious. Time did not permit a more thorough evaluation of this data.

TABLE III. Effect of Sensitizing Agents on  
 $\text{Yb}^{3+}$  Fluorescent Intensity

	$\text{Nd}_2\text{O}_3$	$\text{Yb}_2\text{O}_3$	$\text{Ce}_2\text{O}_3$	Misc. Oxides	$I_{\text{Yb}}$ (970 nm Excitation)	$I_{\text{Yb}}$ (350-700 nm Excitation)	Standard
2396	4	4			0.65	5.8	3.9
2400	4	4	1.9		0.86	5.7	4.2
2500	4	3	1.9		0.58	5.1	4.35
2494	2	3	1.9		0.9	5.0	4.3
2496	3	2	1.9		0.6	4.1	4.1
2502	4	3	1.9	1.0 Cr	0.2	2.3	4.35
2503	4	4	1.9	1.0 Cr	0.23	2.8	4.3
2519	4	4	1.9	0.5 Cr	0.57	6.4	3.9
2518	4	4	1.9	0.25 Cr	0.78	7.6	4.2
2507	4	4	1.9	5 Mn	0.13	0.75	4.3
2509	4	4		1.0 U	0.19	2.65	4.4
2512	4	4	1.9	0.25 U	0.83	7.6	4.2
2513	4	4	1.0	1.0 U	0.66	6.6	4.3
2510	4	4	1.9	1.0 Mo	0.83	6.0	4.3
2511	4	4		1.0 Mo	0.83	6.6	4.5
2505	4	3	1.9	1.0 V	0.11	1.4	4.1

Transmission spectra of these glasses were made to be sure that the desired valence state of the additive ions had been achieved. The MG-2505 glass which was made under oxidizing conditions showed some absorption around 1000 nm indicating the presence of  $V^{4+}$ -ions in addition to the desired  $V^{5+}$ -ions. The  $V^{5+}$ -ions were considered as possible sensitizing agents since they absorb in the ultraviolet and fluoresce in the yellow region of the spectra. The low fluorescent emission of the  $Yb^{3+}$ -ions in this glass could be accounted for by the presence of the  $V^{4+}$ -ions which may produce quenching of the transfer between  $Nd^{3+}$ -ions and the  $Yb^{3+}$ -ions or quenching of the  $Yb^{3+}$ -ion fluorescence directly.

The MG-2507 composition containing manganese was melted under reducing conditions to enhance the formation of  $Mn^{2+}$ -ions. The absorption spectra indicates that the manganese is present primarily as  $Mn^{3+}$ -ions, which probably accounts for the lack of success from this glass.

Based on the  $Yb^{3+}$ -fluorescent emission data obtained when the samples were excited by all wavelengths except the infrared, the most promising candidates for additional sensitization appeared to be  $Cr^{3+}$ -ions and  $U^{6+}$ -ions. A series of clad laser rods was fabricated using cladding glasses based on composition MG-2400 to which was added 0.025-0.25 wt %  $Cr_2O_3$  or 0.1-0.5 wt %  $UO_2$ . Laser measurements were carried out under the same conditions used in the study of the effect of rare earth concentration on cladding efficiency and again several cladding thicknesses were investigated. Curves of cladding glass thickness vs the input energy required to achieve 100 mJ output are shown in Figure 7 and 8 for cladding glasses containing  $Cr_2O_3$  and  $UO_2$  respectively. The data in Figure 7 for the  $Cr_2O_3$ -containing cladding glasses are probably the least accurate of the data presented here due to non-linearity of the slope efficiency curves obtained for these glasses which makes it difficult to determine both threshold and efficiency at low output energies. The results in Figure 7 show no firm correlation between cladding thickness and  $Cr_2O_3$  concentration. These data, such as they are, indicate that best results are obtained for the lowest concentrations of  $Cr_2O_3$ . These results should probably be repeated due to both the difficulties encountered in obtaining the data and the promising low input energies required for a 100 mJ output which are indicated.

The results for the  $UO_2$  containing cladding glasses show better correlation between the cladding glass thickness and  $UO_2$  concentration. That is, all the data indicate that the optimum laser rod configuration for maximum efficiency at 100 mJ output is one which contains 0.1 to 0.2 wt %  $UO_2$  in a cladding

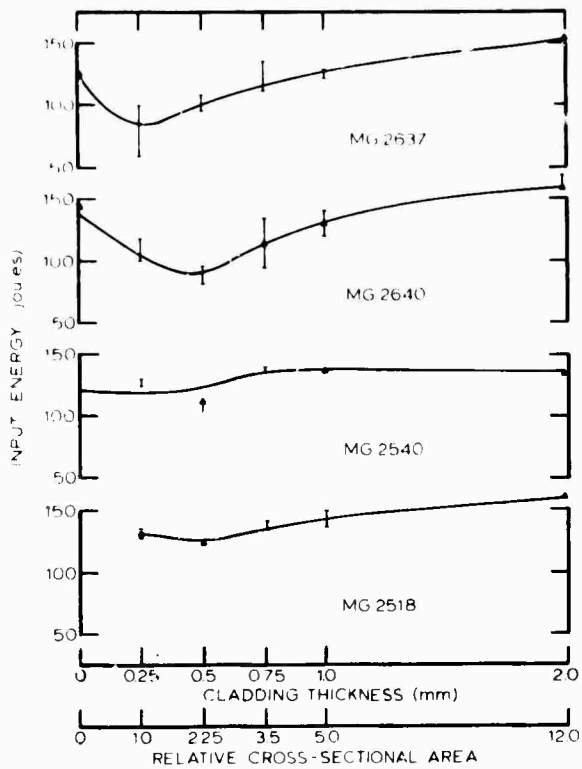


**Figure 7.** Input energy required for 100 mJ output vs cladding thickness of  $\text{Cr}^{3+}$ -cladding glasses.

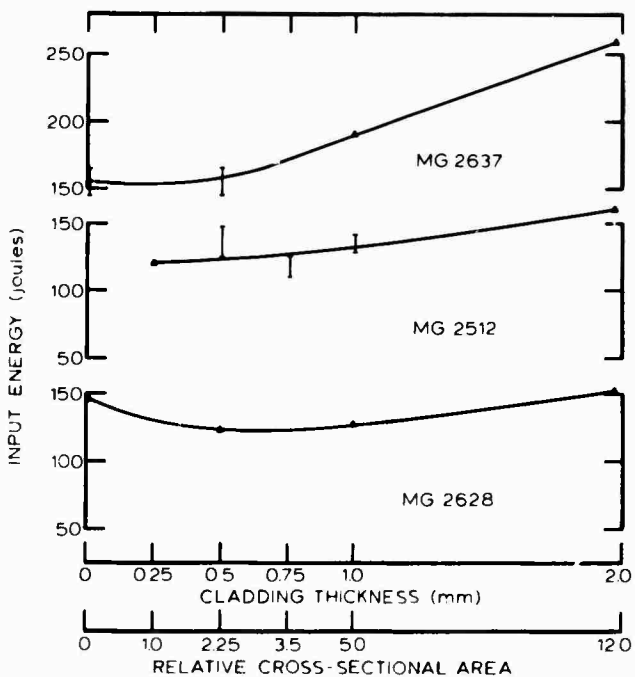


**Figure 8.** Input energy required for 100 mJ output vs cladding thickness of  $\text{U}^{6+}$ -cladding glasses.

thickness of 0.5 to 1 mm for a 4 mm diameter by 76 mm long core.

These results indicate that variations in cladding composition for the core composition and core dimensions used is probably not as significant as the core composition itself.

### 2.3 LASER ROD DIMENSION

Based on the performance of some of the better cladding glasses such as MG-2400 or MG-2512, it would appear that these rods are capable of much higher outputs than is required for the present application. At an input energy twice that of laser threshold, for example, an MG-2512 clad laser rod has an output of 500 mJ or about 10 times the required output. This suggests that lower thresholds might be achieved by using a smaller volume of core glass. To investigate this possibility, a laser rod with a 4 mm core of MG-2101 and a 6 mm OD cladding of MG-2400 was measured to determine the effect on laser performance of making the length of the rod progressively shorter. Results of this work are given in Table IV. In all cases, the arc length of the flashlamp was equal to the length of the laser rod. The dimensions listed under the heading of the flashlamp in Table IV are the inside and outside diameters of the flashlamp envelope.

TABLE IV. Effect of Cavity Parameters  
on Laser Performance

Laser <sup>a</sup> Rod Length (mm)	Flash- <sup>b</sup> lamp (mm)	L	C	Output Mirror	Laser Threshold (joules)	Slope Efficiency	Input at 100 mJ
76	4 x 6	760	4460	65	120	0.51	140
64	4 x 6	"	"	"	115	0.31	150
64	3 x 4	"	"	"	100	0.5	120
50	3 x 4	"	"	"	85	0.31	120
50	3 x 4	"	"	80	75	0.34	105
38	3 x 4	"	"	65	90	0.26	127
38	3 x 4	"	"	"	70	0.29	105
38	3 x 4	"	"	90	~ 45	0.17	105
38	3 x 4	380	"	90	65	0.14	135
38	3 x 4	"	954	90	55	0.07	195

<sup>a</sup>Clad laser with 4 mm core diameter and 6 mm cladding diameter.

<sup>b</sup>Flashlamp envelope dimensions (inside diameter x outside diameter) with arc length equal to the laser rod length.

These limited results indicate in general that considerable improvement in laser performance can be obtained by varying laser rod dimension. In the 50 to 100 mJ output range, the best performance was obtained when the diameter of the flashlamp is slightly less than that of the laser rod, and the volume of the active core material is kept to a minimum, i.e., the shorter laser rods appeared to perform better than longer ones when appropriate end mirrors are used. Changes in the circuit parameters which would tend to shorten the pump pulse had an adverse affect on the output at 100 mJ. This suggests that longer pump pulses should be investigated. Further work is needed in this area before the complete picture of the effect of cavity parameters on laser performance is available.

### 3. Er<sup>3+</sup> SITE STUDIES

#### 3.1 THE EFFECT OF DIFFERENT SITES UPON THE Er<sup>3+</sup> EMISSION SPECTRA IN GLASS

During the work on the previous contract<sup>3</sup> evidence for two erbium sites in a zinc aluminophosphate glass was found. This evidence consisted of the observation of three peaks in the low temperature absorption spectra of the Er<sup>3+</sup>  $^4I_{15/2}$  -  $^4S_{3/2}$  transition. The low temperature of 20°K confined most of the ions to the lowest Kramers doublet in the  $^4I_{15/2}$  ground state. Thus, the peaks observed in the absorption spectra corresponded to the splittings in the upper state which in this case was the  $^4S_{3/2}$  state. From Kramers theorem, it is known that for a single site the  $^4S_{3/2}$  states can split into no more than two Kramers doublets. Thus, the appearance of three distinct peaks shows that there are two sites in the glass. There must also be a fourth absorption band which is masked by the other bands.

The discovery of the three bands in this spectra suggested that the energies of the  $^4S_{3/2}$  levels are extremely sensitive to changes in the Er<sup>3+</sup>-environment. In the other absorption bands, the presence of the extra site resulted in a blurring of the low temperature spectra with a broadening of the lines and filling in of the valleys. Thus, the presence of the extra site was not clearly distinguished in these other spectra.

It is known that the rare earth spectra changes from base glass to base glass. A systematic program was carried out with a few different glasses to see if other sites could be found.

In working with the low temperature  $^2F_{7/2} - ^2F_{5/2}$  absorption and emission spectra of  $Yb^{3+}$  in a series of binary alkali silicate glasses previous to the award of this contract, the  $Yb^{3+}$  spectra was found to change in a systematic fashion with alkali type. As a sequel to that work, it was decided to investigate the  $Er^{3+}$  spectra in these same base glasses. These base glasses were binary alkali silicate glasses of molar composition 33%  $A_2O$  and 67%  $SiO_2$  where A was the alkali ions  $Li^+$ ,  $Na^+$ ,  $K^+$ ,  $Rb^+$ , and  $Cs^+$  unless otherwise noted. Simple glasses were chosen for this investigation to facilitate the interpretation of the results. This molar ratio of alkali to silicate was chosen because this base glass will not phase separate by itself. However, the effect of the rare earth content upon the phase separation of the doped glass is not known.

The different  $Er^{3+}$  sites are illustrated in Figure 9, Curves 1, 2 and 3 which show the low temperature  $^4I_{15/2} - ^4S_{3/2}$  absorption bands for the lithium silicate, potassium silicate, and cesium silicate doped with 4 wt %  $Er_2O_3$ . There were two sites in the lithium silicate glass, Curve 1. The peak at 542.7 nm corresponds to what will be called the B site and the peak at 546.5 nm corresponds to the A site. The central peak at 544.5 is a mixture of the other peaks from each of the two sites.

The potassium glass, Curve 2, shows the A site very clearly with no distinctive peak for the B site in evidence. In Figure 9, Curve 3,  $Er^{3+}$  in the cesium silicate glass exhibits evidence of a third site or, as it will be called, the C site. This site is identified by the peak at 548.7 nm which does not appear for either the A or B sites. The peaks at 544.7 and 546.5 nm correspond to the A site. The position of the second peak of the C site is not known.

The  $^4I_{15/2} - ^4S_{3/2}$  low temperature absorption spectra was also observed in the sodium and rubidium silicate glasses of the molar composition described previously. The former glass with 4 wt %  $Er_2O_3$  showed primarily A sites with a small but observable amount of B site. The binary rubidium silicate glass containing 4 wt %  $Er_2O_3$  showed A sites with a smaller number of C sites than found in the cesium silicate glasses. In short, the  $Na^+$  and  $Rb^+$  glasses showed the progressive changes in the alkali silicate series.

The 548.7 nm  $Er^{3+}$  peak of the C site is very close to the 548.8 nm peak observed by Gruber, Henderson, Muramato, Rajnak and Conway<sup>4</sup> in single crystal erbium oxide. This suggests that the C site may be similar to that in the  $Er_2O_3$  crystal. An

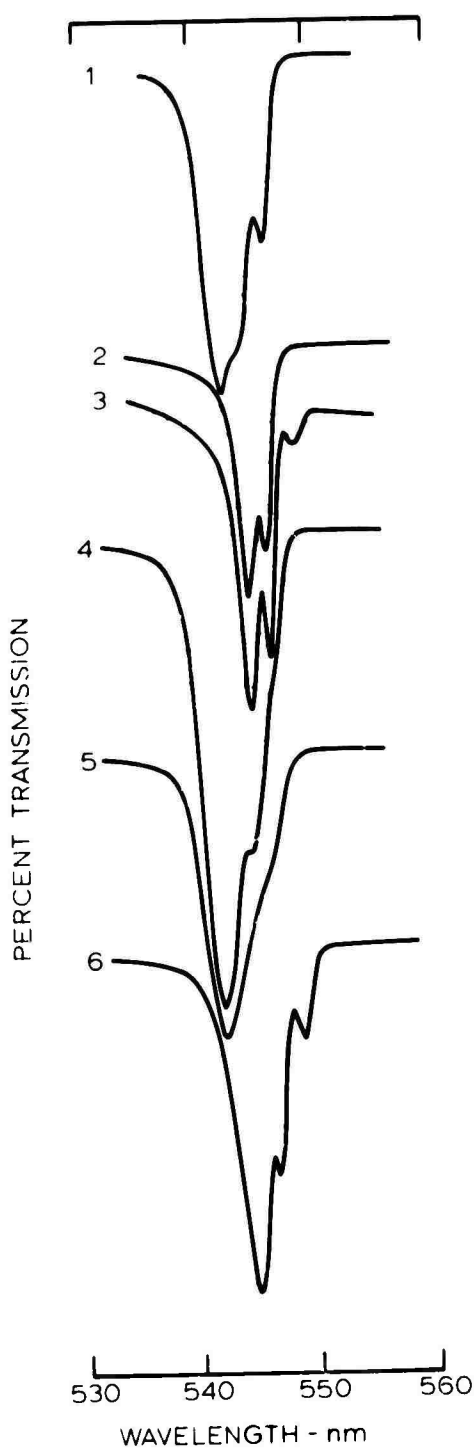


**Figure 9. Low temperature  $I_{15/2}$  -  $^4S_{3/2}$  spectra.**

- (1) 33  $\text{LiO}_2$ , 67  $\text{SiO}_2$ , M% glass, plus 4 wt %  $\text{Er}_2\text{O}_3$
- (2) 33  $\text{K}_2\text{O}$ , 67  $\text{SiO}_2$ , M% glass, plus 4 wt %  $\text{Er}_2\text{O}_3$
- (3) 33  $\text{Cs}_2\text{O}$ , 67  $\text{SiO}_2$ , M% glass, plus 4 wt %  $\text{Er}_2\text{O}_3$
- (4) 33  $\text{LiO}_2$ , 67  $\text{SiO}_2$ , M% glass, plus 50 wt %  $\text{Er}_2\text{O}_3$
- (5) 45 wt %  $\text{SiO}_2$ , 10 wt %  $\text{Na}_2\text{O}$  and 45 wt %  $\text{Er}_2\text{O}_3$  glass
- (6) 62.6 wt %  $\text{Cs}_2\text{O}$ , 26.8 wt %  $\text{SiO}_2$  and 10.6 wt %  $\text{Er}_2\text{O}_3$  glass

examination of the other  $\text{Er}^{3+}$  bands in cesium glass does show some other peaks which correspond to the crystal oxide site. However, the remaining  $\text{Er}^{3+}$  bands characteristic of the cesium silicate glass do not correspond to the crystal oxide spectra. This leaves the identification of the C site as oxide like, somewhat in doubt.

The number of B sites can be increased by decreasing the alkali/rare earth ratio on the lithium and sodium silicate glasses. In Curve 4 (Fig. 9), the low temperature  ${}^4\text{I}_{15/2} - {}^4\text{S}_{3/2}$  absorption spectra is shown for 50 wt %  $\text{Er}_2\text{O}_3$  in the binary lithium silicate glass. The ratio of  $\text{Li}^{1+}/\text{Er}^{3+}$  is 2.50 in this glass. The observed spectra is primarily that of the B site which is showing peaks at 542.2 nm and 544.5 nm. There is a slight bulge in the spectra at 546.5 nm which shows that a small quantity of A sites are also present.

A similar result is shown by Curve 5 (Fig. 9) for a sodium silicate glass with molar composition 73%  $\text{SiO}_2$ , 15.5%  $\text{Na}_2\text{O}$ , and 11.5%  $\text{Er}_2\text{O}_3$ . In this glass the  $\text{Na}^+/\text{Er}^{3+}$  ratio was 1.35.

The C site population can be increased by adding more  $\text{Er}_2\text{O}_3$  to the cesium silicate glass. The maximum amount of rare earth dissolvable in the cesium silicate base glass turned out to be 10 wt %  $\text{Er}_2\text{O}_3$  and the  ${}^4\text{I}_{15/2} - {}^4\text{S}_{3/2}$  spectra in this glass is shown as Curve 6 (Fig. 9). The higher concentration of  $\text{Er}_2\text{O}_3$  has increased the relative populations of the C sites with respect to the A sites as indicated by the stronger peak at 548.6 nm. It is also interesting to note that the 544.7 nm peak intensity has also increased relative to the 546.5 nm peak. It is possible but highly unlikely, that the second peak of the C site underlies this band. This increase in intensity is probably due to the formation of a modified B site in this glass.

The presence of the A, B and C sites also produced changes in the room temperature  ${}^4\text{I}_{13/2} - {}^4\text{I}_{15/2}$  emission spectra. Curve 1 of Fig. 10 shows the  $\text{Er}^{3+}$  emission in the binary lithium silicate base glass. This glass has 15 wt %  $\text{Yb}_2\text{O}_3$ , 0.1 wt %  $\text{Nd}_2\text{O}_3$  to sensitize 0.5 wt %  $\text{Er}_2\text{O}_3$  and is expected to contain a large fraction of B sites. This spectra shows the 1536 nm peak to be greater than the 1543 peak.

Curve 2 of Fig. 10 shows the  $\text{Er}^{3+}$  emission in a potassium silicate glass. The erbium has been sensitized as before with  $\text{Yb}_2\text{O}_3$  and  $\text{Nd}_2\text{O}_3$ . In this spectra the 1536 nm peak and the 1542 nm peak have almost equal intensities. Curve 3 shows a further change in the  $\text{Er}^{3+}$  spectra in the cesium silicate glass. In this glass

the 1542 nm emission peak has become stronger than the 1536 nm emission. The remaining sodium and rubidium silicate glasses possessed spectra that showed the same progressive trend of Figure 10. In Curve 2 (Fig. 10), we see that a pronounced 1.667  $\mu\text{m}$  peak occurs in the potassium glass while this peak is washed out in the lithium and cesium silicate glass, Curves 1 and 3. This is attributed to the extra sites appearing in the last two glasses.

As was demonstrated, the lithium silicate glass possessed a large fraction of B sites, the potassium silicate glass had nearly all A sites and the cesium silicate glass had A sites with a small quantity of C sites and possibly some B sites. We conclude that the presence of B sites enhanced the 1536 nm emission with respect to the 1543 nm emission and that the presence of C sites enhanced the 1543 emission with respect to the 1536 nm emission.

The  $^4I_{13/2} - ^4I_{15/2}$  erbium laser lines are three level systems because the terminal levels are populated at room temperature. From our previous work with low temperature spectroscopy of  $\text{Er}^{3+}$  in a standard silicate laser glass it was found that the 1536 nm emission line terminated on the lowest Stark level in the  $^4I_{15/2}$  ground multiplet. The 1542 nm line terminated on a level about 25  $\text{cm}^{-1}$  above the lowest Stark level.

It should be remembered that the standard laser glass exhibits only A sites and we can discuss this kind of site because the locations of most of the Kramers doublets are known from the low temperature spectroscopy. The B and C site splittings, of course, are different and these crystal field levels have not been located from our present work. Nevertheless it is expected from our experience in the examination of the spectra that the crystal field splittings in the  $^4I_{13/2}$  and  $^4I_{15/2}$  multiplets will be similar to that of the A site. Thus, the following discussion applies in principle to other sites.

In Figure 11, the latest positions of the Kramers doublets for the A site are shown. We see that both the  $^4I_{13/2}$  and  $^4I_{15/2}$  multiplets are split into two groups of levels separated by about 400  $\text{cm}^{-1}$ . The lower group of levels in each J multiplet has an overall separation of about 80  $\text{cm}^{-1}$ . After pumping the ions into the  $^4I_{13/2}$  multiplet, they will quickly reach thermal equilibrium and their distribution in the levels will follow Boltzman statistics. Thus, there will be appreciable population in the lower Kramers doublets with emission occurring from all these levels in the  $^4I_{13/2}$  multiplet into the ground state. Because the periodic spacing of the ground doublets and the excited state doublets are nearly the same and because the levels are not discrete but are homogeneously broadened, the emission at both 1536 nm and

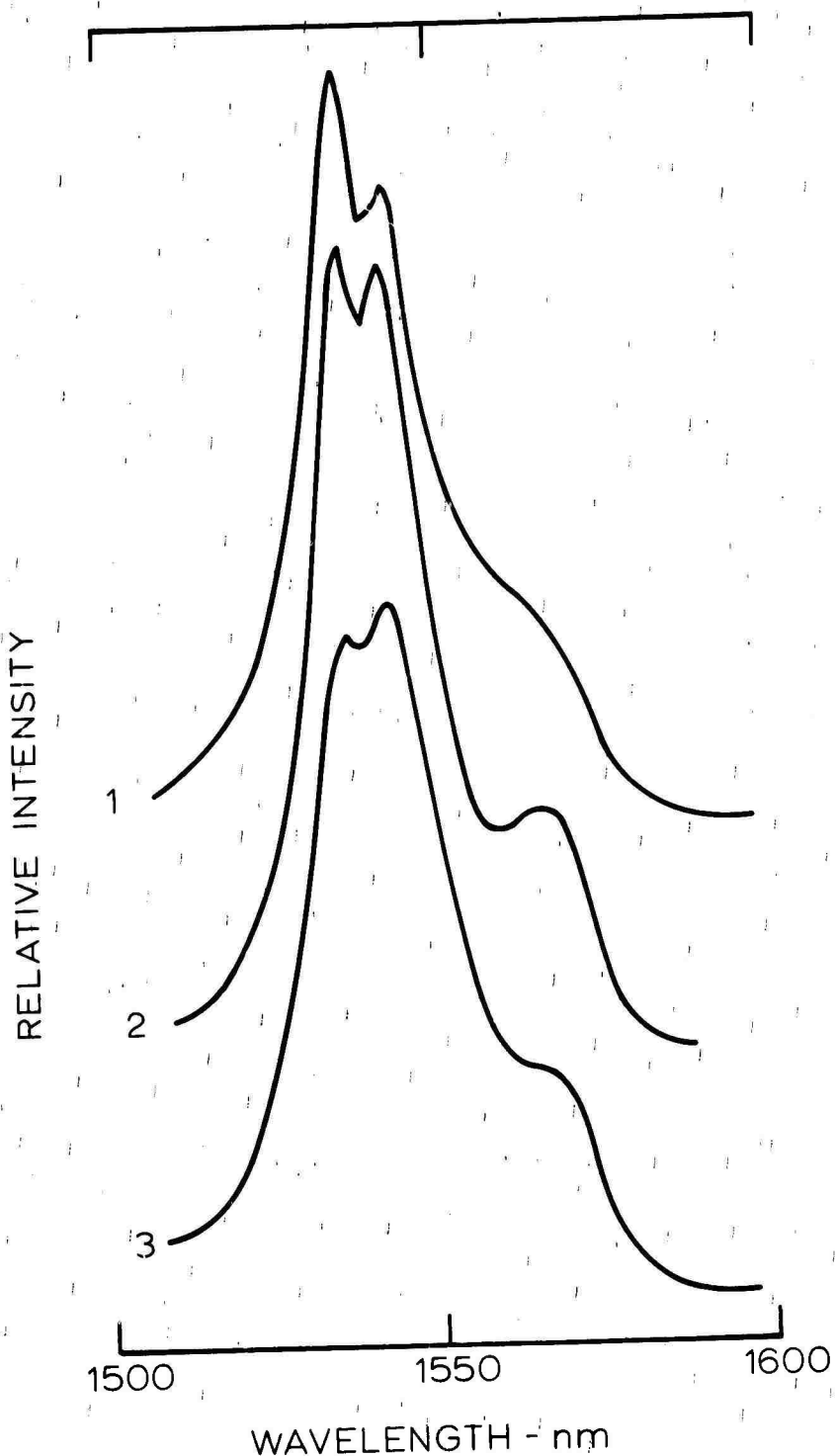


Figure 10. Room temperature  ${}^4I_{13/2} - {}^4I_{15/2}$  emission spectra.

- (1) 33  $\text{Li}_2\text{O}$ , 67  $\text{SiO}_2$ , M% glass, plus 15 wt%  $\text{Yb}_2\text{O}_3$ , 0.5 wt%  $\text{Nd}_2\text{O}_3$  and 0.1 wt%  $\text{Er}_2\text{O}_3$
- (2) 33  $\text{K}_2\text{O}$ , 67  $\text{SiO}_2$ , M% glass, plus 15 wt%  $\text{Yb}_2\text{O}_3$ , 0.1 wt%  $\text{Nd}_2\text{O}_3$  and 0.5 wt%  $\text{Er}_2\text{O}_3$
- (3) 33  $\text{Cs}_2\text{O}$ , 67  $\text{SiO}_2$ , M% glass, plus 15 wt%  $\text{Yb}_2\text{O}_3$ , 0.1 wt%  $\text{Nd}_2\text{O}_3$  and 0.5 wt%  $\text{Er}_2\text{O}_3$

and 1543 nm is the result of transitions between several of the lower lying levels of the  $^4I_{13/2}$  and  $^4I_{15/2}$  multiplets. Thus, the source of the change in these two emission intensity at room temperature becomes complicated because it involves many levels and not just the lowest ones in each multiplet.

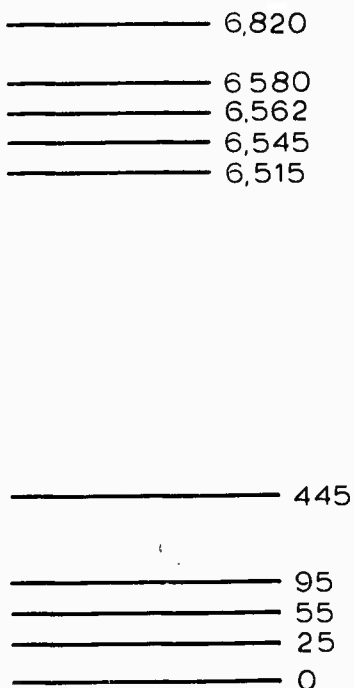


Figure 11. The energies corresponding to the spectral peaks in the  $^4I_{15/2}$  absorption and emission spectra of  $\text{Er}^{3+}$  in the A site.

In Figure 10 the  $\text{Er}^{3+}$  exhibited strong emission at 1536 nm and 1543 nm in all cases. To evaluate the probability of the glass lasing at one vs the other of these wavelengths, the ratio of  $I_{1536} \alpha_{1543}/I_{1543} \alpha_{1536}$  is calculated where I is the fluorescent intensity and  $\alpha$  the absorbance at the specified wavelengths. If this ratio is greater than 1, the glass will lase at the shorter wavelength. Otherwise it operates at the longer wavelength. This is in high Q cavities. The pertinent ratio values are given in Table V.

TABLE V. Merit Factor  $I_{1536} \alpha_{1543}/I_{1543} \alpha_{1536}$   
for Various Glasses

Glass	$\alpha_{1536}/\alpha_{1543}$ ,	$I_{1536}/I_{1543}$	$I_{1536} \alpha_{1543}/I_{1543} \alpha_{1536}$
Curve 1 O	1.48	1.17	0.79
Curve 2 G	1.22	1.00	0.82
Curve 3 E	1.08	0.959	0.89
Curve 1 Q	1.40	1.15	0.820
Curve 2 G	1.69	1.24	0.733
Fig. 14	1.45	1.16	0.800
Fig. 15	1.75	1.29	0.737

However, if the glass is placed in a cavity with end mirrors of low reflectivity, the absorption loss at the two laser wavelengths has a decreased influence on the threshold of the lines. Under these conditions the line with the highest fluorescent intensity will have the lowest pump threshold. Thus, the 1536 nm line would lase in the lithium silicate glass and the 1543 nm line in the cesium silicate glass under these conditions.

### 3.2 GLASSES WITH ENHANCED EMISSION AT 1536 nm

#### 3.2.1 Rare Earth - Silicate Glasses

In our search for evidence of extra sites for  $Er^{3+}$ , a stable soda silicate glass of Figure 9 (curve 5) was formulated with a high concentration of the rare earth. This glass was found to have a large B site population. However, at such high concentrations of  $Er^{3+}$ , the erbium would strongly concentration quench and, therefore, the glass would not be usable as a laser glass. To maintain the high rare earth content and at the same time to prevent the  $Er^{3+}$ -ion from concentration quenching,  $La^{3+}$  and  $Yb^{3+}$  were substituted for the  $Er^{3+}$  (the  $Yb^{3+}$  was a sensitizer for the  $Er^{3+}$  fluorescence). It was, therefore, possible to obtain the strong  $Er^{3+}$  fluorescence shown in Figure 12, Curve 1, for this glass. Apparently there was no strong enhancement of the 1536 nm

line over that of the lithium silicate glass of Figure 10. It is suspected that more of the  $\text{La}^{3+}$  is going into the B sites than the  $\text{Er}^{3+}$  and the  $\text{Er}^{3+}$  is, therefore, not exhibiting a strong B site fluorescent spectrum.

Figure 12, Curve 2, shows that a large component of B site occurs in aluminosilicate glass in that a strong enhancement of the short wavelength emission occurs. The same trick of filling the glass with  $\text{La}^{3+}$  to maintain the high rare earth concentration was used.

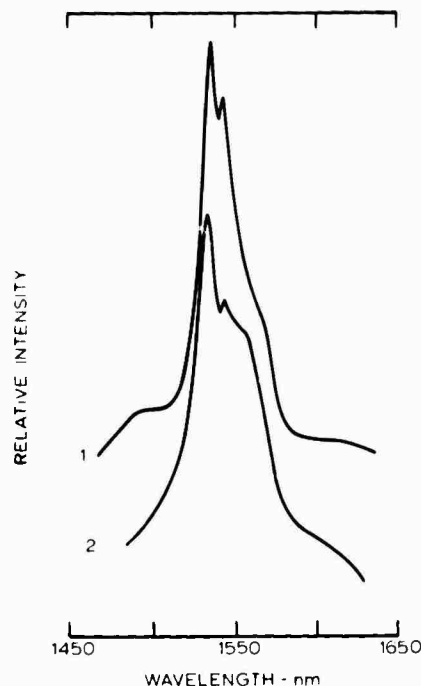


Figure 12. Room temperature  $^4\text{I}_{13/2} - ^4\text{I}_{15/2}$   $\text{Er}^{3+}$  emission spectra .

- (1) 44.5 wt %  $\text{SiO}_2$ , 11.0 wt %  $\text{Na}_2\text{O}$ ,  
28.5 wt %  $\text{La}_2\text{O}_3$ , 14.8 wt %  $\text{Yb}_2\text{O}_3$ ,  
0.2 wt %  $\text{Nd}_2\text{O}_3$  and 1.0 wt %  $\text{Er}_2\text{O}_3$
- (2) lanthanum aluminosilicate glass

### 3.2.2 Phosphate Glasses

A standard ZnO, Al<sub>2</sub>O<sub>3</sub> phosphate laser glass when doped with Er<sup>3+</sup> also exhibited A and B sites as indicated in Figure 13. It should be noted that these peaks do not coincide with those of the silicate glass which is indicative of the difference in the type of base glass. The emission spectra of this glass is shown in Figure 14 where a strong emission at 1534 nm occurred. This enhancement is attributed to the presence of the B sites.

A Ba(PO<sub>3</sub>)<sub>2</sub> glass when doped with Er<sup>3+</sup> exhibited a very large B site population. The Er<sup>3+</sup> emission spectra from this glass in Figure 15 showed the greatest enhancement of the 1533 nm peak that was observed.

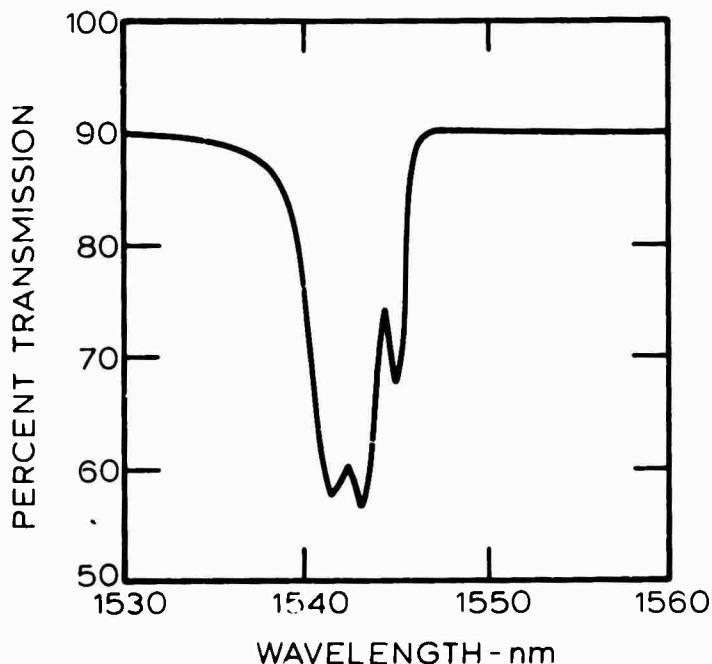


Figure 13. Low temperature  ${}^4I_{15/2} - {}^4S_{3/2}$  Er<sup>3+</sup> absorption spectra in a zinc alumina phosphate glass.

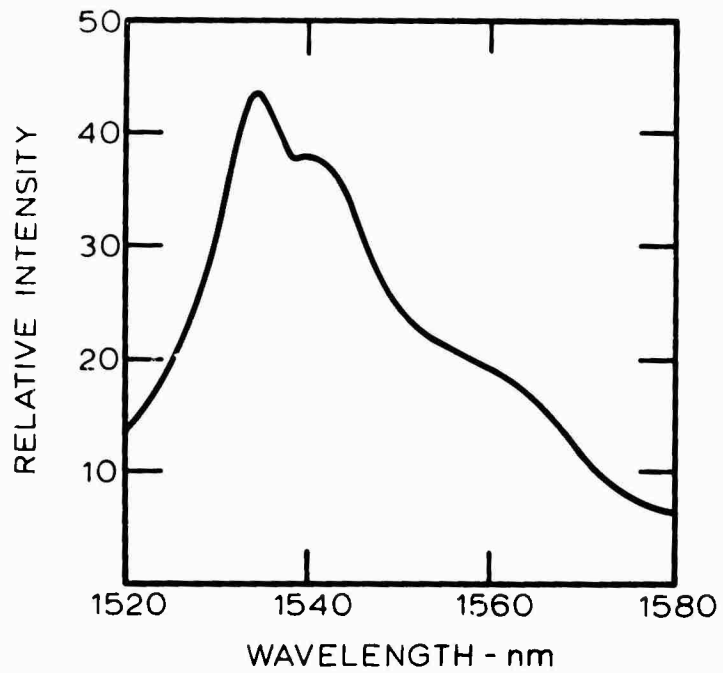


Figure 14. Room temperature  ${}^4\text{I}_{13/2} - {}^4\text{I}_{15/2}$   $\text{Er}^{3+}$  emission spectra in a zinc alumina phosphate glass.

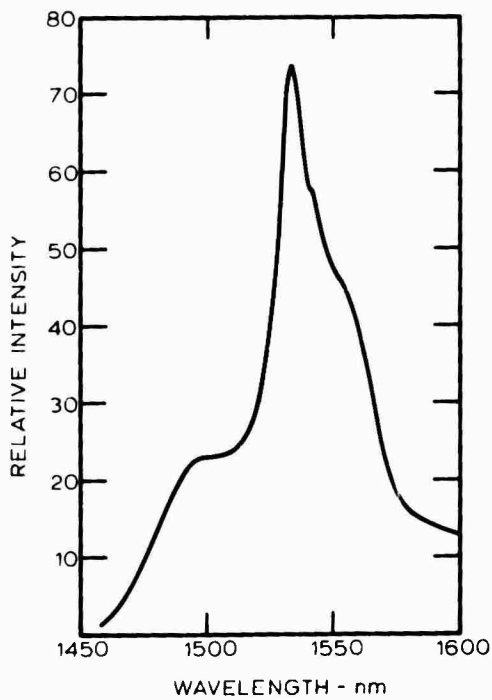


Figure 15. Room temperature  ${}^4\text{I}_{13/2} - {}^4\text{I}_{15/2}$   $\text{Er}^{3+}$  emission spectra in a barium metaphosphate glass.

There are other candidates for strong B site populations. These are the  $\text{NaPO}_3$  and the  $\text{Al}(\text{PO}_3)_3$  glasses as is evidenced from their  $\text{Er}^{3+}$ ,  $^4\text{I}_{15/2} - ^4\text{S}_{3/2}$  low temperature absorption spectrum. Emission samples were not made for these glasses because of time limitations. Their behavior was expected to be similar to that of the  $\text{Ba}(\text{PO}_3)_2$  glass.

### 3.2.3 Germanate and Borate Glasses

A brief evaluation of the site content of the germanate glasses was undertaken. A binary sodium germanate glass was used for the evaluation as this glass was easy to melt over a large range of  $\text{Na}_2\text{O}$  to  $\text{GeO}_2$  concentrations. For a high  $\text{Na}_2\text{O}$  to  $\text{GeO}_2$  molar ratio, the A sites almost completely dominated the spectra as shown in Figure 16, Curve 1, except for the slight bump at 543 nm which indicated a small B site population. By decreasing the  $\text{Na}_2\text{O}$  concentration, the B site population increased rapidly. In Curve 2, Figure 16, for a glass of weight percent concentration of 2.44%  $\text{Na}_2\text{O}$ , 87.56%  $\text{GeO}_2$  and 10%  $\text{Er}_2\text{O}_3$ , the distinguishable peak for the A site at 547 nm was almost completely gone. It was interesting to note that the peak positions in the A and B sites in the germanate glasses rather closely corresponded to those of the silicate glass.

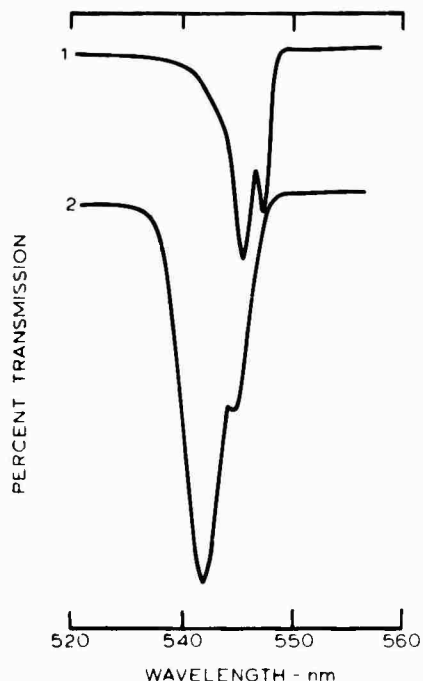


Figure 16. Low temperature  $^4\text{I}_{15/2} - ^4\text{S}_{3/2}$  absorption spectra.  
 (1) 21 wt %  $\text{Na}_2\text{O}$ , 68 wt %  $\text{GeO}_2$   
 and 10.0 wt %  $\text{Er}_2\text{O}_3$   
 (2) 2.44 wt %  $\text{Na}_2\text{O}$ , 87.56 wt %  $\text{GeO}_2$   
 and 10.0 wt %  $\text{Er}_2\text{O}_3$

A short examination was made of the borate glasses where similar multiple sites were found in these glasses. Borate glasses are not considered to be significant laser hosts because the rare earths have very short lifetimes in these glasses.

### 3.3 THE CRYSTAL FIELD SPLITTING OF $\text{Er}^{3+}$ IN THE NEAR OCTAHEDRAL A SITE

Research relevant to this contract, but not performed under it<sup>5</sup> has shown that the peak position of the  $\text{Yb}^{3+}$   $^2\text{F}_{7/2}$  -  $^2\text{F}_{5/2}$  low temperature absorption and emission spectra for silicate glass correspond quite well to the energy level diagrams of Lea, Leask, and Wolf,<sup>6</sup> for a site of octahedral symmetry. This same approach has also been applied to  $\text{Nd}^{3+}$  in barium rubidium silicate glass.<sup>7</sup> This approach has been expanded to take into account the expected trigonal distortion in the A site and has shown that a simultaneous twisting of the three tetrahedra surrounding the  $\text{Yb}^{3+}$  ion predicts the asymmetrical line shapes observed in the  $\text{Yb}^{3+}$  spectra.<sup>8</sup>

The actual rare earth A site is expected to have symmetry  $D_3$ . Thus, a perfect agreement between the Lea, et al diagrams and the observed spectra peaks is not expected. However, in the case of the A sites for  $\text{Yb}^{3+}$  and  $\text{Nd}^{3+}$  a surprisingly good agreement was achieved. In this section, we correlate the crystal field splittings in the J multiplet of the  $^4\text{I}$  term of  $\text{Er}^{3+}$  in silicate glass with an octahedral model for the rare earth site.

The agreement is perhaps not as striking as for the  $\text{Yb}^{3+}$  and  $\text{Nd}^{3+}$ , but it does demonstrate that  $\text{Er}^{3+}$  is in a site whose symmetry is approximately octahedral. The  $\text{Er}^{3+}$  spectra has much more detail than the  $\text{Nd}^{3+}$  spectra and, therefore, small misalignments between the observed peaks and the model are much more apparent. However, it was possible to establish the degeneracy of some of the bands which are not resolved into the underlying Kramers doublets.

The wavefunctions of the high lying  $^4\text{I}_{9/2}$  and  $^4\text{I}_{11/2}$  multiplets of  $\text{Er}^{3+}$  are mixed by intermediate coupling with functions of the same J value from the higher terms. Thus these levels are not pure LS coupled states and the simple procedure of generating the multiplication constants  $\beta$  and  $\gamma$  from the formulas of Elliot, Judd, and Runciman<sup>9</sup> cannot be used. Erath<sup>10</sup> gives these constants for intermediate coupling. In his calculations, he assumed the following electrostatic and spin orbit interaction parameters for erbium:  $F_3 = 433.64 \text{ cm}^{-1}$ ,  $F_4 = 67.522 \text{ cm}^{-1}$ ,  $F_6 = 7.090 \text{ cm}^{-1}$ , and  $\zeta_{4f} = 2471.0 \text{ cm}^{-1}$ . Erath's values of  $\beta$  and  $\gamma$  are given in Table VI.

TABLE VI. Operator Equivalent Factor for Er<sup>3+</sup> (from Erath<sup>1,0</sup>)

Multiplet	$\beta$	$\gamma$
$^4I_{15/2}$	$+ 4.519 \times 10^{-5}$	$1.999 \times 10^{-6}$
$^4I_{13/2}$	$+ 5.655 \times 10^{-5}$	$1.779 \times 10^{-6}$
$^4I_{11/2}$	$+ 4.768 \times 10^{-5}$	$1.739 \times 10^{-6}$
$^4I_{9/2}$	$+ 1.790 \times 10^{-5}$	$3.778 \times 10^{-6}$

The Er<sup>3+</sup> spectra of a standard MG-2084 erbium laser glass which contains mainly A sites, was used for comparison with the octahedral model. The band positions for the  $^4I$  term in this glass were listed in Figure 6 of the final report of the previous contract.<sup>3</sup> The procedure was to fit the band separation of the  $^4I_{9/2}$  multiplet to the diagrams of Lea, et al, for octahedral symmetry. Fitting factors obtained from these diagrams were then used to calculate the crystal field parameters  $A_4\langle r^4 \rangle$  and  $A_6\langle r^6 \rangle$  from which the separation of the energy levels of the remaining  $^4I$  multiplets were determined.\* Good correlation was obtained between these calculations and the observed spectra of the remaining  $^4I$  term as shown in Figures 18-20.

In the  $^4I_{13/2} - ^4I_{15/2}$  emission spectra of Figure 20, the model predicts five long wavelength bands while only four are observable. The calculations indicate that the short wavelength peaks at 1.536 and 1.543  $\mu\text{m}$  are the two Kramers doublets in the  $\Gamma_8^1$  state. The weak band at 1550 nm is probably the single  $\Gamma_7$  state (a better alignment could be obtained between the calculated position and the observed peak by slightly changing the crystal field parameter values). The band at 1.56  $\mu\text{m}$  then becomes the

\*[Assuming the long wavelength peaks of Figure 17 to be associated with a  $\Gamma_8$  state and the short wavelength peak at 792 nm, with the other  $\Gamma_8$  state one obtains fitting factors of  $x = 0.64$  and  $W = 4.56$  which result in crystal field parameter value of  $A_4\langle r^4 \rangle = 273 \text{ cm}^{-1}$  and  $A_6\langle r^6 \rangle = 17.3 \text{ cm}^{-1}$ ].

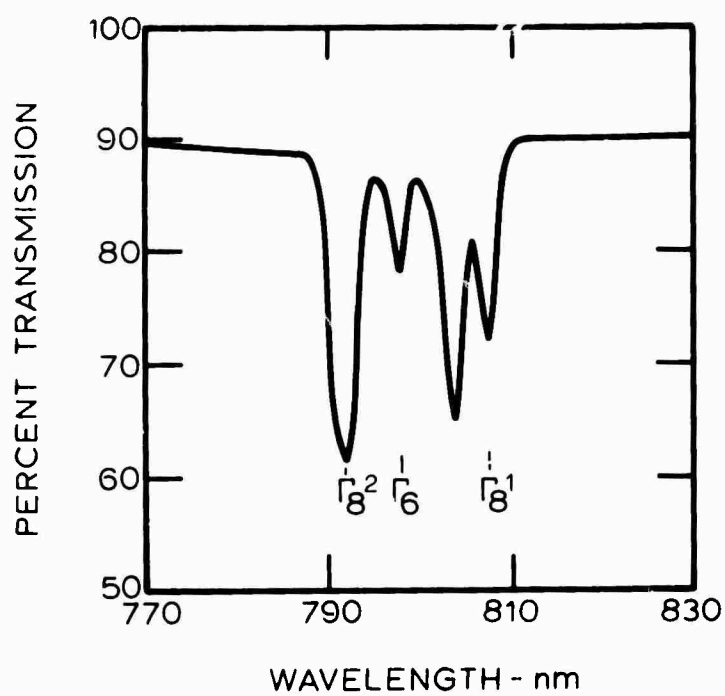


**Figure 17.** The low temperature A site  ${}^4I_{15/2} - {}^4I_{9/2}$   $\text{Er}^{3+}$  absorption spectrum.

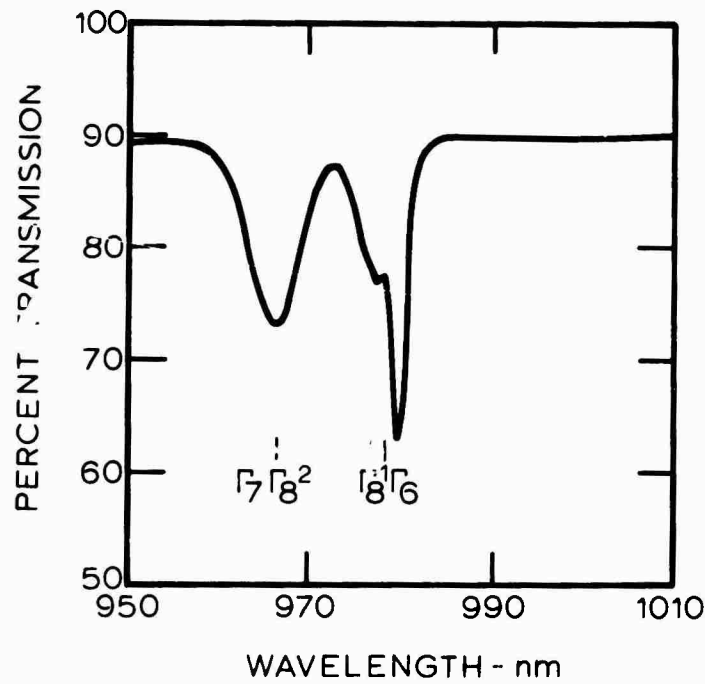


**Figure 18.** The low temperature A site  ${}^4I_{15/2} - {}^4I_{11/2}$   $\text{Er}^{3+}$  absorption spectrum.

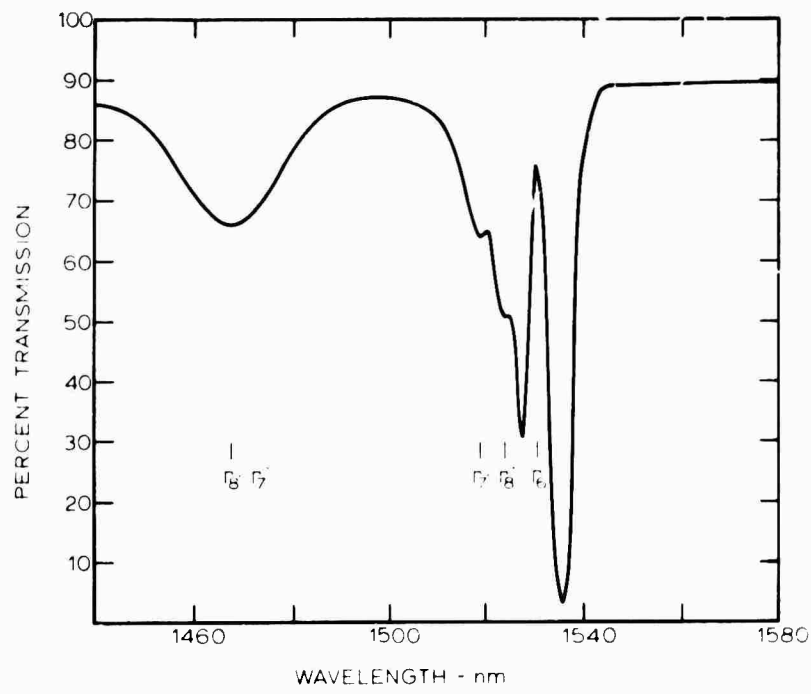


**Figure 19.** The low temperature A site  ${}^4I_{15/2} - {}^4I_{13/2}$   $\text{Er}^{3+}$  absorption spectrum.

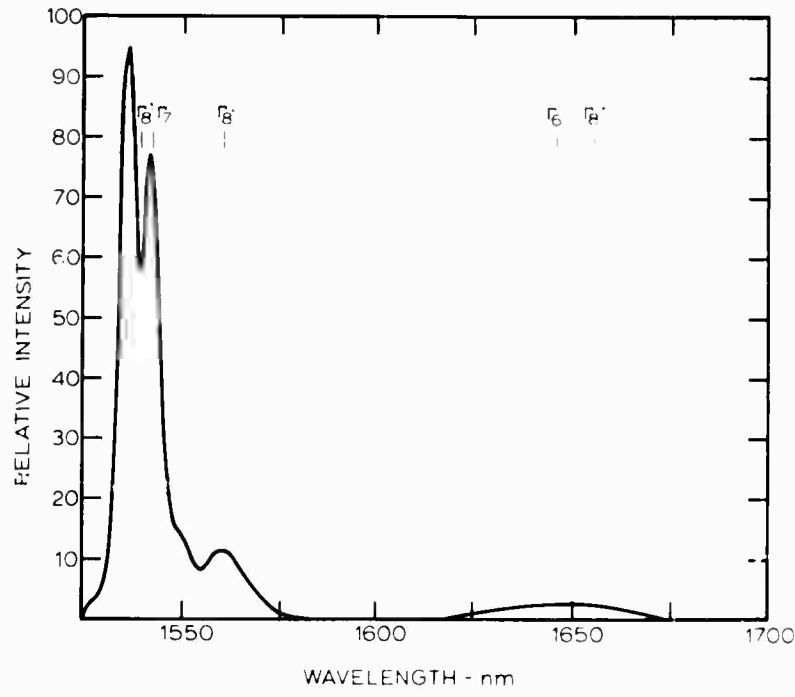


**Figure 20.** The low temperature A site  ${}^4I_{13/2} - {}^4I_{15/2}$   $\text{Er}^{3+}$  emission spectrum.

doubly degenerate  $\Gamma_8$ <sup>2</sup> state. In short, the simplified crystal field analysis places the missing band in the vicinity of 1.56  $\mu\text{m}$ . It should be remembered that because of the presence of lower symmetry components other than cubic, the closely spaced  $\Gamma_8$ ,  $\Gamma_7$ , etc. states will interact with each other in a manner not taken into account by the octahedral model. This interaction will cause these levels to shift with respect to each other and it is by no means certain that the various closely spaced bands can be assigned octahedral state designations as indicated by our calculations. Nevertheless, the so-called doubly degenerate  $\Gamma_8$  states invariably correspond to closely spaced doublets in the observed spectra.

As in the case of the  $\text{Nd}^{3+}$  spectra not all the Kramers doublets were identified in the  $\text{Er}^{3+}$  spectra. However, in all the  $^4\text{I}$  multiplets of  $\text{Er}^{3+}$ , the observed doublets in the low energy bands are all accounted for by the octahedral model. The one exception is the missing band in the  $^4\text{I}_{15/2}$  multiplet.

The  $^4\text{I}$   $\text{Nd}^{3+}$  spectra is inverted with respect to the  $\text{Er}^{3+}$  spectra. For the  $\text{Nd}^{3+}$ , all the Kramers doublets were located in the  $^4\text{I}_{9/2}$  multiplet and in the low energy band of the  $^4\text{I}_{15/2}$  multiplet. (This band corresponds to the high energy band of the  $\text{Er}^{3+}$   $^4\text{I}_{15/2}$ ). A cross correlation of the spectra of the  $\text{Nd}^{3+}$  and  $\text{Er}^{3+}$  shows that the A rare earth site is six-fold coordinated and has near octahedral symmetry.

#### 4. SUMMARY AND CONCLUSIONS

A program has been carried out with the goal of improving the performance of clad erbium laser rods, to investigate the effects on laser performance of; (1) rare earth concentration in the core glass, (2) rare earth concentration in the cladding glass, (3) other additives in the cladding glass and (4) laser rod dimensions. The core glass studies indicate that an improvement in laser performance of about 20% can be achieved by reducing the  $\text{Er}_2\text{O}_3$  concentration to the 0.15-0.2 wt %  $\text{Er}_2\text{O}_3$  level. An additional 20% improvement may be obtained by going to an 80% front reflector in place of the 65% reflector used in the "standard" laser cavity.

Results of the rare earth concentration studies in the cladding glass indicate that an additional 20% improvement in performance can be obtained for a glass containing  $\text{Yb}_2\text{O}_3$  and  $\text{Nd}_2\text{O}_3$  concentrations in the 4.0-5.0 wt % range when a cladding thickness of 0.5 to 0.75 mm is used rather than the 2 mm thickness used on the "standard" laser rod. The investigation of

other additives in the cladding glass indicates that  $\text{CeO}_2$  can be successfully added to the cladding glass to prevent solarization in the rod without affecting the laser performance of the rod. Of the additional sensitizing ions investigated only  $\text{Cr}^{3+}$  and  $\text{U}^{3+}$  showed indications of increasing the  $\text{Yb}^{3+}$  fluorescence from the cladding glass. Results indicate that rather low concentrations of these ions should be added and even in these cases the overall improvement in performance may be marginal. Further investigation is suggested in the case of the  $\text{Cr}^{3+}$ -ion since the slope efficiency curves of all of these glasses were non linear making it difficult to establish threshold and efficiency at low energy outputs.

A somewhat limited investigation of the effect of cavity parameters on laser performance indicate that, in the cavity used, the diameter of the flashlamps should be kept less than that of the laser rod; the 76 mm laser rod length is probably too long; and that longer pump durations should be investigated. The latter conclusions are reached upon rather limited data and the whole study of cavity dimensions should be given much closer attention.

In support of the materials improvement program some work has been done on the "lattice" sites of the  $\text{Er}^{3+}$ -ions in the host glass. In a series of binary alkali silicate glasses three different sites were observed which depend on the alkali element present. In a potassium silicate glass only A-type sites were observed. As progressively lighter alkali ions are used in sodium and lithium, the presence of B-type sites becomes more prevalent and as progressively heavier alkali ions are used, i.e. rubidium and cesium, more C-type sites are observed. The wavelength of the  $\text{Er}^{3+}$  emission varies as a function of the type of sites, i.e., for A-type sites the fluorescent emission intensity at 1536 nm is approximately equal that at 1543 nm, for B-type sites, the 1536 nm emission is enhanced and for C-type sites 1543 nm emission is enhanced. Several glasses were investigated which had enhanced emission at 1536 nm due to the presence of B-type sites, such as rare earth sodium silicate glasses, phosphate glasses, and germanate glasses.

Samples of all of the significant core and cladding combinations investigated under this contract were supplied to the contracting agency. In addition, several samples of some more promising glasses which were melted in ceramic crucibles, thus making them suitable for Q-switched work, were also supplied to the agency.

## REFERENCES

1. D. A. LaMarre and J. P. Segre, "Novel Erbium Q-switched Laser." Proc. of the Fourth DOD Conf. on Laser Technology, p. 1221 (1970).
2. R. F. Woodcock, C. C. Robinson and E. Snitzer, "Er<sup>3+</sup> Glass Laser Materials," *ibid*, p. 1229.
3. R. F. Woodcock, "Multiple Doped Erbium Glasses," Contract No. DAAB07-68-C-0313, Final Report, ECOM-0313-F, Ft. Monmouth, N.J., Oct. 1969, unclassified.
4. J. B. Gruber, J. R. Henderson and M. Muramato, *J. Chem. Phys.* 45, 477 (1966).
5. C. C. Robinson and J. T. Fournier, *J. Phys. Chem. Solids* 31, 895 (1970).
6. K. R. Lea, M.J.M. Leask and W. P. Wolf, *J. Phys. Chem. Solids* 23, 1381 (1962).
7. C. C. Robinson, *J. Chem. Phys.* (In press, 1971).
8. J. T. Fournier and R. H. Bartrum, *J. Phys. Chem. Solids* 31, 2675 (1970).
9. J. P. Elliot, B. R. Judd and W. A. Runciman, *Proc. Roy. Soc. A240*, 509 (1957).
10. E. H. Erath, *J. Chem. Phys.* 34, 1985 (1961).